Journal Pre-proofs

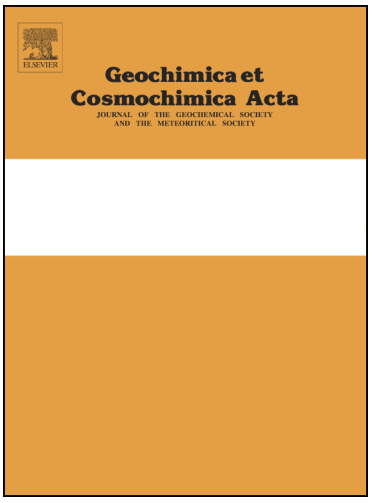


# Glacial controls on redox-sensitive trace element cycling in Arctic fjord sediments (Spitsbergen, Svalbard)

Lisa C. Herbert, Natascha Riedinger, Alexander B. Michaud, Katja Laufer, Hans Røy, Bo Barker Jørgensen, Christina Heilbrun, Robert C. Aller, J. Kirk Cochran, Laura M. Wehrmann

PII: S0016-7037(19)30758-6
DOI: https://doi.org/10.1016/j.gca.2019.12.005
Reference: GCA 11552

To appear in: *Geochimica et Cosmochimica Acta*

Received Date: 10 April 2019
Revised Date: 7 November 2019
Accepted Date: 3 December 2019

Please cite this article as: Herbert, L.C., Riedinger, N., Michaud, A.B., Laufer, K., Røy, H., Barker Jørgensen, B., Heilbrun, C., Aller, R.C., Kirk Cochran, J., Wehrmann, L.M., Glacial controls on redox-sensitive trace element cycling in Arctic fjord sediments (Spitsbergen, Svalbard), *Geochimica et Cosmochimica Acta* (2019), doi: https://doi.org/10.1016/j.gca.2019.12.005

This is a PDF file of an article that has undergone enhancements after acceptance, such as the addition of a cover page and metadata, and formatting for readability, but it is not yet the definitive version of record. This version will undergo additional copyediting, typesetting and review before it is published in its final form, but we are providing this version to give early visibility of the article. Please note that, during the production process, errors may be discovered which could affect the content, and all legal disclaimers that apply to the journal pertain.

© 2019 Published by Elsevier Ltd.

# Glacial controls on redox-sensitive trace element cycling in Arctic fjord sediments (Spitsbergen, Svalbard)

Lisa C. Herbert[1*], Natascha Riedinger[2], Alexander B. Michaud[3+], Katja Laufer[3++], Hans Røy[3], Bo Barker Jørgensen[3], Christina Heilbrun[1], Robert C. Aller[1], J. Kirk Cochran[1], and Laura M. Wehrmann[1]

[1]School of Marine and Atmospheric Sciences, Stony Brook University, Stony Brook, NY, 11794-5000, USA, lisa.herbert@stonybrook.edu, christina.heilbrun@stonybrook.edu, robert.aller@stonybrook.edu, kirk.cochran@stonybrook.edu, laura.wehrmann@stonybrook.edu

[2]Boone Pickens School of Geology, Oklahoma State University, Stillwater, OK, 74078-3031, USA, natascha.riedinger@okstate.edu

[3]Center for Geomicrobiology, Department of Bioscience, Aarhus University, 8000 Aarhus C, Denmark, bo.barker@bios.au.dk, abmichaud@bios.au.dk, katja.laufer@bios.au.dk, hans.roy@bios.au.dk

* Corresponding Author, lisa.herbert@stonybrook.edu

[+] Current address: Bigelow Laboratory for Ocean Sciences, East Boothbay, Maine, 04544 amichaud@bigelow.org

[++] Current address: GEOMAR, Helmholtz Center for Ocean Research, D-24148 Kiel, Germany, klaufer@geomar.de

Declarations of interest: none

Journal Pre-proofs

*Abstract*

Glacial meltwater is an important source of bioessential trace elements to high latitude oceans. Upon delivery to coastal waters, glacially sourced particulate trace elements are processed during early diagenesis in sediments and may be sequestered or recycled back to the water column depending on local biogeochemical conditions. In the glaciated fjords of Svalbard, large amounts of reactive Fe and Mn (oxyhydr)oxides are delivered to the sediment by glacial discharge, resulting in pronounced Fe and Mn cycling concurrent with microbial sulfate reduction. In order to investigate the diagenetic cycling of selected trace elements (As, Co, Cu, Mo, Ni, and U) in this system, we collected sediment cores from two Svalbard fjords, Van Keulenfjorden and Van Mijenfjorden, in a transect along the head-to-mouth fjord axis and analyzed aqueous and solid phase geochemistry with respect to trace elements, sulfur, and carbon along with sulfate reduction rates. We found that Co and Ni associate with Fe and Mn (oxyhydr)oxides and enter the pore water upon reductive metal oxide dissolution. Copper is enriched in the solid phase where sulfate reduction rates are high, likely due to reactions with $H_2S$ and the formation of sulfide minerals. Uranium accumulates in the solid phase likely following reduction by both Fe- and sulfate-reducing bacteria, while Mo adsorbs to Fe and Mn (oxyhydr)oxides in the surface sediment and is removed from the pore water at depth where sulfidization makes it particle-reactive. Arsenic is tightly coupled to Fe redox cycling and its partitioning between solid and dissolved phases is influenced by competition with FeS for adsorption sites on crystalline Fe oxides. Differences in trace element cycling between the two fjords suggest delivery of varying amount and composition of tidewater glacier (Van Keulenfjorden) and meltwater stream (Van Mijenfjorden) material, likely related to oxidative processes occurring in meltwater streams. This processing produces a partially weathered, more

Journal Pre-proofs

reactive sediment that is subject to stronger redox cycling of Fe, Mn, S, and associated trace elements upon delivery to Van Mijenfjorden. With climate warming, the patterns of trace element cycling observed in Van Mijenfjorden may also become more prevalent in other Svalbard fjords as tidewater glaciers retreat into meltwater stream valleys.

*1. Introduction*

In high latitude regions, the sub- and proglacial environment is an important zone of physical and chemical (biotic and abiotic) weathering of bedrock which provides a significant source of trace elements to the ocean (e.g. Anderson et al., 1997; Mitchell et al., 2001, 2006; Raiswell et al., 2006; Statham et al., 2008; Bhatia et al., 2013; Hawkings et al., 2014, 2018). Polar ocean productivity is thought to be limited by the availability of iron (Fe) and other bioessential trace elements such as cobalt (Co), nickel (Ni), and copper (Cu), and therefore changes in glacial supply of these elements may have implications for primary productivity and associated global biogeochemical cycles (Morel et al., 1991; Cullen, 2006; Nielsdóttir et al., 2009; Sunda, 2012; Rijkenberg et al., 2018). Many trace elements have a low solubility in seawater and accumulate in marine sediments, where they undergo biogeochemical transformations and are subsequently sequestered in the solid phase or recycled back to the water column (Morel and Price, 2003; Cid et al., 2012; Charette et al., 2016; Kondo et al., 2016).

The behavior of trace elements in sediments is controlled by early diagenetic processes, mainly the redox changes associated with remineralization of organic matter. Remineralization can affect trace element behavior by generating metabolic products (e.g. $Mn^{2+}$, $Fe^{2+}$, and $H_2S$) that react with the trace elements or by changing the ambient oxidation state and causing reductive/oxidative dissolution or precipitation (Shaw et al., 1990; Calvert and Pedersen, 1993;

Achterberg et al., 1997; Morford and Emerson, 1999; Algeo and Maynard, 2004; Tribovillard et al., 2006). During dissimilatory reduction of Fe and Mn (oxyhydr)oxides (-OHO), trace elements associated with the Fe- and Mn-OHO, such as Co, Ni, and arsenic (As), are released to the pore water along with $Fe^{2+}$ and $Mn^{2+}$; conversely, the precipitation of Fe and Mn as oxide, carbonate, or sulfide minerals can remove these trace elements from the pore water through adsorption or co-precipitation (Canfield, 1989; Burdige, 1993; Nameroff et al., 2004; Audry et al., 2006; Tapia and Audry, 2013; Monien et al., 2014; Riedinger et al., 2014). During microbial sulfate reduction, the production of $H_2S$, formation of sulfide minerals, and oxidation of sulfides can serve to sequester or release trace elements such as Cu and molybdenum (Mo) (Huerta-Diaz and Morse, 1992; Helz et al., 1996; Morse and Luther III, 1999; Brumsack, 2006). Additionally, some trace elements such as uranium (U) may be reduced or oxidized directly by microbes (Lovley, 1993). Thus, the biogeochemical fate (sequestration or transport) of each trace element is largely controlled by relative rates of Mn, Fe, and S reduction-oxidation in the sediment during early diagenesis.

Iron and manganese cycling in Svalbard fjord sediments is fueled by a large supply of reactive Fe- and Mn-OHO delivered in glacial meltwater (Kostka et al., 1999; Nickel et al., 2008; Wehrmann et al., 2014). Previous studies have suggested that dissimilatory metal oxide reduction may contribute 10-26% to the total organic matter remineralization in Svalbard fjords (Kostka et al., 1999), and 69-90% to anaerobic carbon mineralization in the top 10 cm of sediment in the Barents Sea east of Svalbard (Vandieken et al., 2006). Sulfate reduction is also an important metabolic pathway in these sediments, with rates comparable to those of temperate shelf sediments (Glud et al., 1998; Sagemann et al., 1998; Kostka et al., 1999). The Svalbard fjord deposits near glacial outlets are impacted by non-steady state conditions at the sediment

water interface related to episodic changes in organic carbon supply and sediment accumulation rate related to seasonality in glacial meltwater pulses and spring/summer phytoplankton blooms (Hop et al., 2002; Svendsen et al., 2002). Additionally, the sediments can experience physical mixing by bioturbating organisms (Glud et al., 1998) and, in shallow water depths, are frequently disturbed by iceberg ploughing and rapid formation and/or slumping of bedforms such as deltas around meltwater stream outlets or push moraines at the terminus of surging glaciers (Zajączkowski et al., 2004; Forwick et al., 2009; Farnsworth et al., 2017; Hodal et al., 2012; Hegseth and Tverberg, 2013; Kempf et al., 2013; Lalande et al., 2016). Given the asymmetry of a typical fjord system from head (glacier-influenced) to mouth (ocean-influenced), the fjords show strong gradients in physical, chemical, and biological characteristics along the head-to-mouth axis (Hop et al., 2002; Svendsen et al., 2002; Bourgeois et al., 2016). These dynamic conditions exert tight control over the distribution and rates of dissimilatory metal reduction and sulfate reduction, which often occur in the same depth horizons of sediment (Buongiorno et al., 2019). The balance between Fe and S cycling is related to relative inputs of organic carbon and glacial material.

Before delivery to the fjord, glacial material is physically and chemically altered beneath the glacier and, in the case of land-terminating glaciers, during transport between the glacial terminus and the fjord (e.g. Hodson et al., 2008). In the subglacial zone of small, polythermal valley glaciers such as those on Svalbard, comminution of bedrock produces glacial flour with a high surface area to volume ratio, which can serve as a substrate for both microbial activity and inorganic weathering reactions (Bottrell and Tranter, 2002; Tranter et al., 2002; Wadham et al., 2004, 2010; Wynn et al., 2006; Montross et al., 2012). Rock-water reactions and active subglacial microbial communities produce $CO_2$ that enhances the dissolution of carbonate and

silicate bedrock (Tranter et al., 2003). Pyrite oxidation, a particularly important reaction in these systems (Tranter et al., 2003), generates protons for further bedrock dissolution, adds chemolithoautotrophic energy for the base of the microbial food web, and consumes oxygen to allow other redox reactions such as Mn and Fe reduction (Sharp et al., 1999; Hodson et al., 2008; Wadham et al., 2010; Boyd et al., 2014; Nixon et al., 2017). There is evidence for active subglacial microbial communities beneath several glaciers in close proximity to fjords examined in this study (Wadham et al., 2004; Kaštovská et al., 2007). Van Keulenfjorden is fed by several polythermal, surge-type tidewater glaciers that deliver glacial sediment directly from the glacier either through subglacial discharge or iceberg rafting. Many of the glaciers feeding Van Mijenfjorden, in contrast, have retreated such that their termini are now located on land and glacial sediment is transported to the fjord through proglacial meltwater streams. Sediment transported in these streams is likely subject to weathering reactions such as carbonate dissolution, sulfide oxidation, and cation denudation, adding another processing step before release of subglacial material into the fjord (Chillrud et al., 1994; Anderson et al., 2000; Wadham et al., 2001; Cooper et al., 2002).

The aim of this study is to investigate the interactions between trace element behavior and the cycling of C, S, Fe, and Mn in surface sediments of Van Mijenfjorden and Van Keulenfjorden, and how these processes are controlled by glacial input. The Arctic regions are particularly sensitive to warming associated with anthropogenic climate change (Spielhagen et al., 2011; Larsen et al., 2014), and glaciers throughout the polar regions, including Svalbard, are melting rapidly (Dowdeswell et al., 1997; Ziaja, 2001; Kohler et al., 2007; Bliss et al., 2014; Zemp et al., 2019). As a result of glacial retreat, land-terminating glaciers and meltwater streams are expected to become more prevalent. We aim to understand how such a shift from direct

subglacial discharge (e.g. Van Keulenfjorden) to meltwater stream input (e.g. Van Mijenfjorden) may influence the trace metal cycling, sequestration, and transport in glacially impacted fjords.

*2. Study area and sampling sites*

Svalbard is an archipelago in the northwest Barents Sea between 77 and 80° N, with a total land area of 63,000 $km^2$ (Hjelle, 1993). The fjords investigated in this study—Van Mijenfjorden and Van Keulenfjorden— are located on the western coast of Spitsbergen, the largest and westernmost island in the Svalbard archipelago. The fjords are geographically adjacent, and share similar catchment area geologies (Table 1; Fig. 1). The bedrock surrounding both fjords is dominated by Helvetiafjellet and Carolinefjellet formations, members of the Adventdalen Group that date to the Early Cretaceous and are comprised mainly of shales, siltstones, and sandstones, with some carbonate beds and hydrocarbon-rich layers (Dallmann, 1999). The Van Mijenfjorden Group is also prevalent around both fjords— these Paleocene/Eocene formations consist of shales, siltstones, and sandstones with seams of coal. Many of these formations are marine in origin and contain minerals such as glauconite, siderite, dolomite, clay ironstone, and pyrite. Van Keulenfjorden may also be influenced by the Sassdalen, Kapp Toscana, Janusfjellet, and Tempelfjorden groups from the Triassic, Jurassic, and Permian. These shale-siltstone-sandstone formations are exposed on the southwestern shore of Van Keulenfjorden, and include bituminous shale, limestone, and chert (Dallmann, 1999).

Svalbard land area is 60% covered by ice sheets and glaciers and the landscape is dominated by glacial erosion, with little soil and vegetation (Hjelle, 1993; Onarheim et al., 2014). The west coast of Spitsbergen is influenced by relatively warm Atlantic water of >3°C carried by the West Spitsbergen Current north from the Gulf Stream to the Arctic Ocean

Journal Pre-proofs

(Svendsen et al., 2002). The fjords on the western coast of Spitsbergen, including Van Mijenfjorden and Van Keulenfjorden, are ice-free for much of the year and their circulation is largely driven by the intrusion of deep, warm (>3° C) Atlantic water under a fresh, cold (~1° C) surface layer from glacial meltwater (Svendsen, et al., 2002; Cottier et al., 2005; Cokelet et al., 2008).

Van Mijenfjorden is the longer and wider of the two fjords, and is fed primarily by an extensive meltwater stream from Kjellströmdalen, which forms the northern branch at the head of the fjord (Fig. 1). The southern branch of the fjord is fed by a small tidewater glacier called Paulabreen that is currently retreating, and may have surged between 250 and 600 years ago (Rowan et al., 1982). A second large meltwater stream system drains into the northern, central part of the fjord through Reindalen. The circulation of the deep water in and out of this fjord is partially restricted by Akseløya, a narrow island across the mouth of the fjord (Hjelle, 1993). Three sites were selected for coring in Van Mijenfjorden: an inner site located near the mouth of the Kjellströmdalen meltwater stream system (VM-In), a middle site (VM-Mid), and an outer site located on the fjord side of Akseløya (VM-Out) (Table 1; Fig. 1).

Van Keulenfjorden is located south of Van Mijenfjorden, and fed by two tidewater glaciers at the head: Nathorstbreen and Doktorbreen. Nathorstbreen is a polythermal glacier that surged between 2008 and 2016 (Fig. 1; Sund and Eiken, 2010; Kempf et al., 2013; Lovell et al., 2018). This surging behavior affects sediment transport into the fjord, and past surges in Van Keulenfjorden and other fjords can be inferred from distinct sediment lobes on the seafloor (Kempf et al., 2013). A shallow (30 m depth) sill at the mouth impedes the intrusion of Atlantic water into the fjord, and the fjord is further divided into inner and outer basins by submarine moraines (Kempf et al., 2013). Three sites were selected for coring (Table 1; Fig. 1): an inner

site within the inner basin (VK-In), and middle (VK-Mid) and outer (VK-Out) sites within the outer basin. The VK-In site is located close (within 4 km) to the calving front of the surging Nathorstbreen and is likely influenced by heavy sedimentation from glacial activity. VK-Mid is located near the shore at the outlet of the land-terminating glacier Penckbreen, and within the delta bedform created by meltwater stream input from Penckbreen (Kempf et al., 2013). VK-Out is located near the sill at the fjord mouth.

## *3. Methods*

### *3.1 Sample collection*

Sediment cores were collected at the stations described above during a sampling expedition in early August 2016, aboard the MS *Farm*. These same stations have been cored during previous sampling campaigns, and geochemical datasets from all six sites are available for comparison with the results of the current study (Brüchert et al., 2001; Arnosti and Jørgensen, 2006; Robador et al., 2009; Canion et al., 2014; Wehrmann et al., 2014, 2017). The station names used in these other studies are given in Table 1.

Sediment cores were retrieved using a Rumohr gravity corer (Meischner and Rumohr, 1974) and core liners that were 60-80 cm long and pre-drilled for pore water sampling. Pore water was collected by attaching trace metal-free plastic syringes to Rhizon samplers (Seeberg-Elverfeldt et al., 2005; Dickens et al., 2007). The Rhizon filtration pore size is 0.2 μm, which defines the operational cutoff for dissolved solutes in this study. Pore water aliquots were preserved with zinc acetate (2%, w/v) for sulfate concentration measurements, nitric acid (2%, v/v) for trace element analyses, and stored headspace-free for dissolved inorganic carbon (DIC) analysis. Solid sediment samples were collected from separate Rumohr cores with pre-drilled

holes using cut-off syringes of 1.5 cm diameter and immediately frozen. At the inner sites of both fjords a third core was extruded for $^{210}$Pb analysis, and subsamples were stored at 4°C in plastic bags. Sampling resolution for pore water and solid sediment in all Rumohr cores was 2 cm in the top 20 cm, 4 cm over the next 40 cm, and 8 cm below 60 cm.

Samples for sulfate reduction rate (SRR) measurements were collected with a Haps corer (Kanneworff and Nicolaisen, 1983). The Haps core was subsampled using 2.5 cm diameter subcores with ports drilled down the length of the subcore at 1 cm resolution and filled with gas-impermeable polyurethane (Sikaflex-11FC). Subcoring was carried out using an active suction device to avoid compaction of the sediment.

*3.2 Radionuclide analysis*

Samples from separate cores were extruded from the core barrel and sliced, then dried and powdered for radionuclide analysis. Measurements of $^{210}$Pb, $^{226}$Ra, and $^{137}$Cs were made by gamma spectrometry using a Canberra 3800 mm$^2$ LeGe (low energy germanium) gamma detector, counting for 3-7 days per sample. $^{210}$Pb and $^{137}$Cs were determined using the 46 keV and 661 keV peaks, respectively, while $^{226}$Ra was measured using the 352 keV $^{214}$Pb peak. $^{210}$Pb activities were corrected for self-absorption. Unsupported $^{210}$Pb was calculated by subtracting the background $^{226}$Ra from the total $^{210}$Pb. Precisions for $^{210}$Pb, $^{226}$Ra, and $^{137}$Cs analyses were 4.8%, 1.5%, and 13% respectively. Precision is calculated throughout as the averaged percent relative standard deviations of replicate sample measurements. The sediment accumulation rate was estimated using three different methods. First, we assumed that the depth of disappearance of unsupported $^{210}$Pb (43 at VM-In) was equivalent to 5 half-lives of $^{210}$Pb, or ~110 years. Using the second method, we considered the sediment accumulation rate to be the decay constant of $^{210}$Pb

(-0.0311 $s^{-1}$) divided by the slope of the best-fit line of the natural log plot of unsupported $^{210}Pb$. Finally, the $^{137}Cs$ peak (~30 cm at VM-In) was assumed to correspond with the year 1964, the date of maximum bomb-derived radionuclide fallout in the Northern Hemisphere (Ritchie and McHenry, 1990).

*3.3 Sulfate reduction rate analysis*

Subcores for SRR analyses were stored at in situ temperature (2°C) for up to 3 days until radiotracer injection. The overlying water was removed immediately before radiotracer injection began, and the stopper replaced on the top of the core tube. Five microliters of 50 kBq, carrier-free $^{35}SO_4^{2-}$ was injected with a glass syringe through the polyurethane ports at 1 cm resolution down core. The core was then incubated at in situ temperature (2°C) for 14 h. After incubation, the cores were extruded and sliced at 1 cm intervals. The 1 cm sediment intervals were immediately placed in 10 ml of 10% zinc acetate and homogenized thoroughly with a vortex mixer, then frozen at -20°C.

The $^{35}SO_4^{2-}$ reduced during incubation was recovered from FeS, $FeS_2$, and $S^0$ by cold chromium distillation and trapped in 5 mL of 5% zinc acetate as $Zn^{35}S$ (Røy et al., 2014). The $Zn^{35}S$ and $^{35}SO_4^{2-}$ was quantified separately using liquid scintillation counting and the sulfate reduction rate was calculated according to Jørgensen (1978). Sulfate reduction rate was calculated in nmol $cm^{-3}$ $d^{-1}$ using measured porosity (from 0.8 in surface samples to 0.5 at depth; data not shown). Earlier precision tests of the $^{35}S$-method have shown a relative standard deviation in homogenized sediment of ±6% (Jørgensen, 1978), which is smaller than the variation in rates observed here due to sediment heterogeneity.

*3.4 Solid phase analyses*

Sediment samples were homogenized, dried, powdered, and analyzed for total carbon (TC) and total nitrogen (TN) contents using a CNS Elemental Analyzer (Thermo EA1112). Aliquots of the powdered samples were acidified with 6 M HCl in a sealed reaction chamber, and the change in pressure due to the release of $CO_2$ was measured (Jones and Kaiteris, 1983). The change in pressure was related to the total inorganic carbon (TIC) concentrations via a calibration curve generated by measuring the pressure change following dissolution of known masses of pure calcium carbonate. Because of drying, grinding, and extensive exposure to oxygen, FeS was likely only present in small quantities in some samples relative to the TIC content, so the pressure of released hydrogen sulfide gas was negligible in this analysis. Total organic carbon (TOC) was calculated as the difference between TC and TIC. Carbon to nitrogen ratios (C/N) were calculated on a mol/mol basis using the total organic carbon and total nitrogen contents. The precisions for total N, total C, and TIC analyses were 4.3%, 1.1%, and <1% respectively.

Frozen solid sediment was analyzed for acid volatile sulfide (AVS) and chromium reducible sulfur (CRS) content by a two-step distillation following the method described by Fossing and Jørgensen (1989). Prior to any solid-phase analyses, sediment in contact with the plastic core liner that may have been smeared or oxidized was discarded. Samples were digested in a closed distillation system in cold 6 M HCl for 1 hour followed by a boiling acidic 0.5 M $CrCl_2$ solution for 2 hours. The released sulfide from AVS and CRS was trapped in separate vials containing 5% zinc acetate solution. The ZnS concentration in the traps was determined using the Cline spectrophotometric method (Cline, 1969). The precisions for the AVS and CRS analyses were 34% and 9%, respectively. The high uncertainty in the AVS measurement is likely

due to the extremely low concentrations in some samples, and possibly to uneven distribution of FeS in each sample. All solid phase sulfur data are reported in μmole sulfur per gram sediment dry weight.

Further samples of frozen sediment were digested following a sequential extraction adapted from Tessier et al. (1979) and Poulton and Canfield (2005) (Table 2). This extraction was applied to determine the partitioning of trace elements (As, Co, Cu, Fe, Mn, Mo, Ni, and U) between five operationally defined fractions: exchangeable (1 M $MgCl_2$), acid-soluble (1 M sodium acetate adjusted to pH 4.5 with acetic acid), easily reducible (1 M hydroxylamine · HCl), reducible (50 g/L dithionite buffered with sodium citrate), and oxidizable (8.8 M $H_2O_2$). The exchangeable fraction includes trace metals adsorbed onto particle surfaces, and possibly any associated with highly reactive monosulfides inadvertently oxidized during sample handling. The acid-soluble fraction includes elements released from carbonate and the remaining acid-volatile sulfide (such as iron monosulfides) (Tessier et al., 1979; Poulton and Canfield, 2005). Hydroxylamine · HCl is assumed to target amorphous iron minerals like ferrihydrite and lepidocrocite, while dithionite dissolves goethite, hematite, and akagenite, among other similar more crystalline Fe minerals (Poulton and Canfield, 2005). The oxidizable step targets organic matter and incompletely oxidizes pyrite, possibly dissolving ~40% of solid sulfides (Tessier et al., 1979; Gleyzes et al., 2002; Cappuyns et al., 2007; Torres et al., 2013).

The solid samples (0.5-1 g) were homogenized in 10 mL of extractant, and following each step of the extraction, the samples were centrifuged at 4000 rpm for 7 minutes and aliquots were collected for further analysis. All solutions were prepared immediately prior to extraction, and were trace metal grade except for the dithionite, which was only available as reagent grade (Table 2). Reagent blanks were analyzed and used to determine the detection limit for each

element. Extracts were analyzed on an Agilent 7500cx quadrupole inductively-coupled plasma mass spectrometer (ICP-MS) following 1:30 dilution in trace metal-grade 2% $HNO_3$. Standards were prepared from Fluka stock solutions, diluted with trace metal-grade 2% $HNO_3$, and matrix-matched with 30% of each extraction reagent. A trace metal-grade 2% $HNO_3$ blank was run between each sample to monitor the machine background throughout the analysis. Reproducibility was determined by repeated analyses of a frozen in-house standard sediment that was subjected to the sequential extraction simultaneously with the samples. The reproducibility, given as percent relative standard deviation, averaged ~12% across all analyzed elements and reagents (see Supplemental Table S1). All solid phase trace element data are reported based on dry sediment weight.

*3.5 Pore water analyses*

Pore water was analyzed for sulfate and chloride using ion chromatography (IC) on a Metrohm 930 Compact IC system with matrix elimination (3.2 mM $Na_2CO_3$/1 mM $NaHCO_3$ eluent). Zinc acetate-fixed samples were diluted 1:280 and analyzed in random order. Standards were prepared from Metrohm certified stock solutions (1000 ppm), and IAPSO seawater was analyzed as an external standard. Sulfate and chloride concentrations were calculated using dilution factors obtained from the measured acetate concentration and the known concentration of the zinc acetate solution used to preserve the pore water samples. The precision for the sulfate and chloride measurements was 2.3%.

Dissolved inorganic carbon ($\Sigma CO_2 = CO_2 + HCO_3^- + CO_3^{2-}$) concentration was measured using a flow injection analysis (FIA) system based on conductivity detection following Hall and Aller (1992). Standards were prepared from reagent grade $NaHCO_3$, and the conductivity

response was linear over the relevant concentration range (~1-15 mM DIC). A new standard curve was created every two hours to account for drift associated with changes in the ambient temperature and pressure. Precision for DIC analysis was 6%. Carbonate concentrations for the calculation of carbonate mineral saturation indices were obtained using the program $CO_2$Sys version 2.1, with the following input parameters: salinity = 35, temperature = 4° C, pressure = 1010 dbars, and pH = 7.5 (NBS scale).

Concentrations of pore water trace elements (As, Co, Cu, Fe, Mn, Mo, Ni, and U) were analyzed by ICP-MS using a Thermo Fisher iCAP Qc at Oklahoma State University. Standards were prepared with addition of NaCl in 2% trace metal grade $HNO_3$ to match the pore water matrix of the diluted samples. The pore water samples were diluted 25-fold with 2% trace metal grade $HNO_3$ and analyzed in random order. A standard reference material (NIST SRM 1643f in a 2% NaCl matrix) was run with each batch as a quality control, and machine drift was corrected for using an internal standard run along with the samples. Accuracy was calculated as the percent difference between the average of six separate measurements of the standard and the certified concentrations for each element (Supplemental Table S2). The analytical precision was determined as the percent relative standard deviations of more than ten repeated measurements of prepared standards and sample replicates, and was better than 5% for all elements (Supplemental Table S2).

## *4. Results*

### *4.1 Radionuclide distribution*

At the inner site in Van Mijenfjorden, the calculated sediment accumulation rates are high—0.58 cm year$^{-1}$ based on the depth of the $^{137}$Cs peak, 0.61 cm year$^{-1}$ based on the natural log of

the unsupported $^{210}$Pb profile, and 0.4 cm year$^{-1}$ based on the depth of unsupported $^{210}$Pb disappearance (Fig. 2a-c). At the inner site in Van Keulenfjorden, a sediment accumulation rate could not be calculated as the values of unsupported $^{210}$Pb and $^{137}$Cs are low relative to the other site and show no significant depth trend. (Fig. 2d-e). The $^{137}$Cs peak was not found within the recovered sediment; however, we can calculate a minimum net accumulation rate of 1.1 cm year$^{-1}$ if the bottommost sample (which contained the highest concentration of $^{137}$Cs recovered at this site) is assumed to represent 1964, the year of maximum $^{137}$Cs release. This rate can be considered a minimum because it is likely that the true $^{137}$Cs peak at this site is deeper than 57 centimeters below the sea floor (cmbsf).

*4.2 Sulfate reduction rates*

Sulfate reduction rates at the inner sites average 0.3 nmol $SO_4^{2-}$ cm$^{-3}$ day$^{-1}$, and the values increase strongly with distance from the glacier to an average of 12.3 nmol $SO_4^{2-}$ cm$^{-3}$ day$^{-1}$ at VM-Out and 13.6 nmol $SO_4^{2-}$ cm$^{-3}$ day$^{-1}$ at VK-Out (Fig. 3). Areal rates of sulfate reduction (integrated over the top 14 cm of each core) also demonstrate the increases with distance from the glacier in both fjords, with rates of 6.1 nmol cm$^{-2}$ d$^{-1}$, 29.1 nmol cm$^{-2}$ d$^{-1}$, and 263 nmol cm$^{-2}$ d$^{-1}$ at VK-In, -Mid, and -Out, respectively, and 2.3 nmol cm$^{-2}$ d$^{-1}$, 41.1 nmol cm$^{-2}$ d$^{-1}$, and 193 nmol cm$^{-2}$ d$^{-1}$ at VM-In, -Mid, and -Out, respectively. Sulfate reduction rates generally increase with depth in the sediment at all sites with the exception of the outer stations, which have peaks between 3-12 and 2 – 4 cmbsf for VM and VK, respectively (Fig. 3).

*4.3 Solid phase carbon, nitrogen, sulfur, and trace element composition*

The TOC content in both fjords is between 0.4 and 3.0 wt. % with differences of <1 wt % between the averages of the sites (Table 3; Supplemental Figure S1). The average C/N ratios (in mol $mol^{-1}$) in the fjords range from 20.4 ± 0.5 at the inner site to 16.4 ± 1.4 at the outer site in Van Mijenfjorden and from 18.7 ± 1.5 (VK-In) to 17.8 ± 1.0 (VK-Out) in Van Keulenfjorden (Table 3).

Fe-monosulfide contents, measured as acid-volatile sulfide (AVS), are very low at both inner sites, with an average of 0.01 μmol $g^{-1}$ at VM-In and 0.02 μmol $g^{-1}$ at VK-In (Fig. 4b, e). In both fjords, AVS content increases with distance from the glacier and with depth at each site, reaching maxima of 17.1 μmol $g^{-1}$ at 43 cmbsf at VM-Out and 20.1 μmol $g^{-1}$ at 60 cmbsf at VK-Out (Fig. 4b, e). In Van Keulenfjorden, contents of chromium-reducible sulfur (CRS; $FeS_2$ and $S^0$), predominantly pyrite, are highest (up to 75 μmol $g^{-1}$) in the inner and middle sites, and show no consistent trends with depth at any sites except for a general decrease with depth at the outer site (Fig. 4f). The CRS contents in the inner and middle sites in Van Mijenfjorden are roughly a third of those at the corresponding sites in Van Keulenfjorden (Fig. 4c).

Total extractable solid Fe contents (calculated as the sum of all fractions) average 15 ± 3 mg $g^{-1}$, with 47-70% in the reducible (dithionite) fraction (Fig. 5). There is a slight decrease in the reducible Fe contents with distance from the glacier, with averages of 64% of the total extractable Fe at the inner sites and averages of ~55% at the outer sites in both fjords. Acid-soluble (sodium acetate) Fe shows a slight increase with distance from the glacier and with depth at the middle and outer sites in both fjords. Additionally, the Fe in the acid-soluble fraction that is attributable to Fe in AVS (AVS-Fe; assumed stoichiometry FeS) increases from average values of 0.03% (VM) and 0.06% (VK) at the inner sites to averages of 11% (VM) and 9% (VK) at the outer sites. The percent of AVS-Fe in the acid-soluble fraction also increases with depth,

with the largest values in each fjord of 41% at 39 cmbsf at VM-Out and 20% at 76 cmbsf at VK-Out. Solid phase Fe enrichments in the easily reducible (hydroxylamine · HCl) and reducible fractions are observed in the uppermost 5 cm at the middle and outer stations in both fjords (Fig. 5b-c, e- f). In the exchangeable ($MgCl_2$) fraction, Fe is not present above the detection limit (Supplemental Table S2).

Total extractable solid phase Mn contents range from 0.13 to 1.5 mg $g^{-1}$, with the highest contents in the acid-soluble fraction (Fig. 6; 22%-72% of the total). Compared to the high percentage of Fe in the reducible fraction, contents of Mn in the reducible fraction are low, 9% to 45% of the total extractable Mn. Distinct solid phase enrichments in the surface sediments at the middle and outer sites are visible predominantly in the acid-soluble phase the uppermost 2 cm (Fig. 6b-c, f).

In both fjords, Co and Ni show solid phase surface enrichments primarily in the reducible fraction (Figs. 7 and 8). The exchangeable fraction accounts for up to 14% and 17% of the total solid contents of Co and Ni, respectively, with overall higher exchangeable contents in Van Keulenfjorden (Figs. 7 and 8). Both Co and Ni have higher oxidizable contents in Van Keulenfjorden than Van Mijenfjorden (Figs. 7 and 8). Overall there is more Ni in the solid phase (Fig. 8; average 15.2 μg $g^{-1}$) than Co in the solid phase (Fig. 7; average 8.6 μg $g^{-1}$).

Solid phase Cu is predominantly (38% to 60% of the total) in the acid-soluble fraction, with 10%-25% in the easily reducible and 14%-39% in the reducible fractions (Fig. 9). At the middle and outer stations of both fjords, a Cu enrichment in the acid-soluble and reducible fractions is visible in the uppermost 10 cm (Fig. 9b-c, e-f).

Solid phase U is primarily in the exchangeable fraction (44 - 70% of the total extractable) at all sites except VM-In and VM-Mid, where it is divided between the acid soluble (34 – 46% of

total) and reducible (~26% of total) fractions (Fig. 10). The percentage of solid U in the exchangeable fraction increases moving away from the glacier in both fjords, while the percentages in all the other fractions decrease. The total extractable U also increases with distance from the glacier in both fjords, with averages from 0.13 μg $g^{-1}$ at VK-In and 0.10 μg $g^{-1}$ at VM-In to 0.41 μg $g^{-1}$ at VK-Out and 0.25 μg $g^{-1}$ at VM-Out (Fig. 10). The percentage of solid U in the exchangeable fraction also generally increases with depth, particularly in the outer sites where it reached maxima of 0.48 μg $g^{-1}$ at 39 cmbsf at VM-Out and 0.60 μg $g^{-1}$ at 12 cmbsf at VK-Out (Fig. 10).

The average total extractable contents of Mo are 1.3 μg $g^{-1}$ at VK-In and -Mid, and 2.2 μg $g^{-1}$ at VM-In (Fig. 11a, d-e). At these three sites, solid phase Mo is primarily in the reducible fraction (~62% of total), and Mo contents show no significant variability over depth, similar to both the solid Fe and Mn profiles (Fig. 11a, d-e). At VM-Mid, VM-Out, and VK-Out, solid phase Mo is strongly partitioned between the surface ~4 cm and the deeper sediment, with higher concentrations in the easily reducible and reducible fractions at the surface and lower concentrations at depth relative to the concentrations at VK-In, VK-Mid, and VM-In (Fig. 11c, e-f). There is a significant contribution of oxidizable Mo to the total amount of Mo at all sites (4% - 25% of total); in the acid-soluble fraction Mo is absent.

Solid phase As is primarily in the reducible fraction (Fig. 12; 56-88% of total extractable As). Surface enrichments in solid phase As are visible in VM-Mid, VM-Out, and VK-Out (Fig. 12b-c, f). These enrichments are largely in the reducible phase, but in the outer sites there are also higher As contents in the easily reducible and acid-soluble fractions relative to the inner sites (Fig. 12a, d). Due to high background levels of As in the magnesium chloride solution, As

concentrations in the exchangeable fraction are below detection limit in nearly all of the samples. The oxidizable fraction contains low but measurable (0.002 – 0.2 μg $g^{-1}$) As concentrations.

*4.4 Pore water chloride, sulfate, inorganic carbon, and trace element concentrations*

At all sites, chloride concentrations stay constant with depth at ~ 530 - 540 mM (seawater value ~ 550 mM; Supplemental Figure S2). At the middle and outer sites of both fjords, pore water sulfate concentrations decrease by 0.5 - 4.1 mM below the typical seawater value (~28.2 mM) over the depth of the core (Fig. 4a, d). At both of the inner sites, pore water sulfate increases over the depth of the core by 1.1 - 1.3 mM above the surface value (Fig. 4a, d). Decreases in DIC are observed at VM-In from 2462 μM in the uppermost sample to a minimum of 510 μM at 41 cmbsf (Supplemental Table S3). All other sites show increases in DIC with depth from ~2000-3000 μM in the surface to 7000-9000 μM at depth (data not shown).

At the inner site in Van Mijenfjorden, dissolved Fe concentrations increase below 5 cmbsf, peaking at 1460 μM at 40 cmbsf, while the middle and outer sites show an increase in the surface 0-20 cm, then reach a constant concentration in deeper sediment regions (300-400 μM) (Fig. 5a-c). The inner site in Van Keulenfjorden, in contrast, has low dissolved Fe concentrations (0-16 μM) in the top 0-50 cm, with an increase to 282 μM at the bottom of the core (Fig. 5d). The maximum concentrations at the middle and outer sites are 655 μM at 19 cmbsf and 359 μM at 12.5 cmbsf, respectively (Fig. 5e-f). At the inner site in Van Mijenfjorden, dissolved Mn shows a large peak of 780 μM at 9 cmbsf (Fig. 6a). At the middle site, there is a small peak of 112 μM at 2 cmbsf depth followed by a gradual increase to values of 89-93 μM below 55 cm depth (Fig. 6b). At the outer site, dissolved Mn concentrations increase from 22 to 46 μM over the top 10 cm and remain relatively constant below (Fig. 6c). In Van Keulenfjorden, the pore

water Mn profile has a peak of 160 μM around 16 cmbsf at the inner site, and a peak of 259 μM at 5 cmbsf depth at the middle site (Fig. 6d-e). At the outer site in Van Keulenfjorden, the surface sample (~0.5 cmbsf) has the highest concentration of pore water Mn with 70 μM, below which concentrations remain between 20 and 36 μM (Fig. 6f).

Pore water Co and Ni peaks are nearly aligned with pore water Mn peaks at all sites, with maximum concentrations of 0.090-0.340 μM for Co and 0.11-0.23 μM for Ni in the topmost 5 cm at the middle and outer sites of both fjords (Figs. 7 and 8). At VK-In and VK-Mid, pore water Co and Ni peaks also align with the pore water Fe peaks at 60 cmbsf and 23 cmbsf, respectively (Figs. 7 and 8, d-e). At VM-In, the decrease in pore water Co and Ni below the Mn reduction zone is not as steep as the decrease in pore water Mn (Figs. 7a, 8a). Ni is below detection limit in the pore water below 31 cmbsf at VK-Mid and below 11 cmbsf at VM-Mid (Fig. 8b, e), while at the outer sites it is below detection limit by 23 cm at VK-Out and by 9 cm at VM-Out (Supplemental Table S2; Fig. 8c, f).

Pore water Cu is above the detection limit (0.14 nM) at both inner stations, but with higher concentrations in Van Mijenfjorden— up to 0.5 μM in VM-In and 0.3 μM in VK-In (Supplemental Table S2; Fig. 9a, d). The observed pore water Cu concentrations at VK-In, VM-In, and VM-Mid are well above Arctic seawater values (Fig. 9a-b, d; 0.005 μM average, 0.017 μM maximum; Tovar-Sánchez et al., 2010). Pore water Cu is also well above seawater values at VM-Mid, with an average concentration of 0.2 μM (Fig. 9b). At VM-Out, dissolved Cu is at the detection limit (Fig. 9c). In Van Keulenfjorden, pore water Cu is present at low concentrations (average 0.3 μM) in the upper 12 cm at the middle site and in the upper 6 cm at the outer site (Fig. 9e-f). The Cu concentration profiles are variable at all sites with concentrations above the detection limit.

There is a decrease in pore water U with depth at all fjord stations except VK-In (Fig. 10). Pore water concentrations in the surface sediments (~0.006 μM) are lower than seawater values based on the salinity of the deep water in the fjords (0.014 μM; Ku et al., 1977) and decrease to values of 0.001-0.003 μM at depth (Fig. 10). The inner site in Van Keulenfjorden was the only location to exhibit an increase in pore water U with depth, from 0.008 μM at the surface to ~0.016 μM below 40 cm depth (Fig. 10d).

The surface sediment at most sites contains pore water Mo concentrations ranging from average seawater concentration (0.122 μM; Tovar-Sánchez et al., 2010) down to ~0.09 μM (Fig. 11). At VM-In, VK-In, and VK-Mid, pore water Mo is removed within and just below the pore water Mn peak to 0.03-0.05 μM (Fig. 11a, d-e). At VM-In and VK-Mid, Mo is released within the pore water Fe peak (37 cmbsf at VM-In and 27 cmbsf at VK-Mid) with maximum concentrations of 0.2 μM at VM-In and 0.25 μM at VK-Mid (Fig. 11a, e). Below the surface peaks (uppermost 2-6 cm) in pore water Mo at VK-Out, VM-Mid, and VM-Out, Mo is steadily removed from the pore water down to seawater value or slightly lower (Fig. 11b-c, f).

Arsenic is released into the pore water in the zone of Fe release at all sites, with low surface pore water concentrations between 0.01 and 0.08 μM and increasing to maximum concentrations of 0.71 μM at depth (Fig. 12). At the inner sites, the maximum dissolved As concentration is 0.21 μM and 0.12 μM in the deepest sample at VM-In and VK-In, respectively (Fig. 12a, d). At the outer sites, the As maxima are 0.71 μM at 35 cmbsf in VM-Out and 0.61 μM at 12.5 cmbsf in VK-Out (Fig. 12c, f). At the middle and outer sites, dissolved As remains high or increases at depth, below ~40 cm depth (Fig. 12b-c, e-f).

## *5. Discussion*

*5.1 Fjord physical dynamics*

Scatter in the unsupported $^{210}$Pb and $^{137}$Cs profiles from VM-In (see Fig. 2) is likely influenced by non-steady state sediment accumulation in the fjord. This profile may also suggest vertical mixing at this site, most likely caused by bioturbation— glacial activity is unlikely to physically impact the sediments of Van Mijenfjorden given the distance between the glacier terminus and the fjord. Similar evidence of non-steady state conditions, mixing, and high sediment accumulation rate was observed in $^{210}$Pb and $^{137}$Cs profiles from Van Mijenfjorden and other Svalbard fjords (Mitchell et al., 1999).

The sediment accumulation rate calculated at VK-In (1.1 cm year$^{-1}$) is likely to be an underestimate given that the true $^{137}$Cs peak (if present) may be much deeper than the bottom of the core. Although the accumulation rate at this site could not be reliably calculated, the variable small quantities of excess $^{210}$Pb (~0.5 dpm g$^{-1}$) and $^{137}$Cs (~0.2 dpm g-1) with no clear depth trend in either parameter across the depth of the core suggest rapid deposition of old material underexposed to atmosphere with intermittent mixing of more recently exposed particles containing excess $^{210}$Pb and $^{137}$Cs (Appleby and Oldfield, 1978; Ritchie and McHenry, 1990; Crusius and Anderson, 1995). This rapid sediment deposition and mixing in Van Keulenfjorden may have been caused by the recent surge of the tidewater glacier Nathorstbreen and the associated increase in sediment discharge, iceberg scouring, and bedform formation and slumping (Solheim and Pfirman, 1985; Gilbert et al., 2002; Sund and Eiken, 2010; Kempf et al., 2013; Lovell et al., 2018). The middle site in Van Keulenfjorden (VK-Mid) also shows evidence of disturbance or rapid sedimentation in the uppermost 10-20 cm, based on $^{210}$Pb and the $^{137}$Cs data collected during the same sampling cruise by Buongiorno et al. (2019). This disturbance at VK-Mid could have been caused by the surge of Nathorstbreen, or sediment input from the

meltwater stream of Penckbreen, a land-terminating glacier near the sampling site (Fig. 1). Based on a recent swath bathymetry map of the seabed in this fjord, we estimate that our sampling site VK- Mid lies near the edge of a delta, and thus may be subject to the same rapid sedimentation or bedform slumping that affects VK-In (Kempf et al., 2013). Although we did not analyze $^{210}$Pb and $^{137}$Cs at the middle or outer sites, the sediment accumulation rates in both fjords likely decrease from head to mouth of the fjord given that the primary source of sediment is the glacier at the head. Such head-to-mouth sedimentation gradients have been previously observed in other fjords on Svalbard (Svendsen et al., 2002; Zaborska et al., 2006; Szczuciński et al., 2009).

Given that the pore water chloride concentrations at all sites in both fjords are roughly constant and close to seawater value (Supplemental Figure S2), it is likely that the deep water in the fjords is well-mixed and sourced from intruding North Atlantic Deep Water, while fresh water from glacier melt flows out of the fjord as a stratified surface layer (see Section 2). Thus, despite the restrictive sills at the fjord mouths and the freshwater glacier influence, the bottom water salinity at all sites appears to be similar.

*5.2 Carbon-driven Sulfur Biogeochemistry*

At the inner fjord sites, sulfate reduction rates are very low and little accumulation of AVS is observed in the sediment (Fig. 3; Fig. 4). At the outer sites in both fjords, increases in both sulfate reduction rates and AVS contents at depth (Figs. 3 and 4b, e) suggest that with higher sulfate reduction rates, more hydrogen sulfide is subsequently trapped as Fe-monosulfide minerals (Canfield, 1989). At these sites we also observed decreases in pore water sulfate with depth that could not be explained by a change in salinity (Supplemental Figure S2); rather, the

sulfate depletions are further indication of removal of sulfide to AVS following sulfate reduction (Jørgensen, 1977; Canfield, 1989).

We suggest that the cross-fjord (head-to-mouth) trend of increasing sulfate reduction rates with distance from the glacier is primarily controlled by the availability (here defined as the concentration per unit volume of sediment) and reactivity of organic carbon in the sediments (Jørgensen, 1982, 1977). At all sites in Van Keulenfjorden and Van Mijenfjorden, the total organic carbon (TOC) contents are in a similar range; however, the ratios of organic carbon to nitrogen (C/N) indicate that the organic carbon source changes across the fjords (Table 3). Terrestrial organic matter has a higher C/N (>20) compared to marine (6-9) organic matter, driven by the C/N of marine phytoplankton (~6.6) (Redfield, 1934; Müller, 1977; Prahl et al., 1980; Meyers, 1990; Schmidt et al., 2010). Bulk terrestrial OC, particularly ancient or petrogenic material, is less bioavailable; thus, sediments with an OC pool containing a greater terrestrial component is expected to have lower rates of remineralization (Hedges and Keil, 1995; Hedges et al., 1997; Prahl et al., 1997). Our observed C/N values indicate a contribution of bulk terrestrial organic matter to the total carbon pool at all sites, which is in good agreement with values obtained in previous studies in Svalbard fjords (10-30; Kim et al., 2011; Bourgeois et al., 2016; Cui et al., 2016; Koziorowska et al., 2016). Decreasing C/N ratios with distance from the glacier in both fjords suggest higher contents of labile, marine OC, primarily marine phytoplankton, near the mouth of the fjord. Other studies have found similar marine OC increases near the mouths of other Spitsbergen fjords based on carbon isotopes and lipid biomarkers (Kim et al., 2011; Kuliński et al., 2014; Bourgeois et al., 2016; Cui et al., 2016; Koziorowska et al., 2016).

Journal Pre-proofs

An increase in pore water sulfate concentration with depth at the inner site in Van Mijenfjorden (Fig. 4a, d) indicates an additional source of sulfate to the system, which could be the oxidation of detrital sulfide minerals such as pyrite. The pyrite pool likely contains a large detrital component in both fjords, given that contents of chromium-reducible sulfur (i.e. pyrite) are highest closest to the glacier and exhibit no increases at the sites with higher sulfate reduction and AVS concentration (Fig. 4c, f). Glacially-derived detrital pyrite is delivered to the Svalbard fjord sediments from glacial erosion (Brüchert et al., 2001; Wehrmann et al., 2014, 2017), and microbial and abiotic processes in the subglacial and proglacial environment can accelerate the weathering and oxidation of pyrite grains in bedrock (Chillrud et al., 1994; Sharp et al., 1999; Montross et al., 2012; Harrold et al., 2016). In marine sediments, pyrite can be oxidized by nitrate, $MnO_2$, and in some cases Fe(III)-OHO (Luther et al., 1982; Aller and Rude, 1988; Schippers and Jørgensen, 2002), and in the Svalbard fjords these oxidants are delivered at high rates in glacial melt, potentially allowing the pyrite oxidation to proceed through both biotic and abiotic pathways using both oxygen and metal oxides as oxidants in the sediments (Wehrmann et al., 2014, 2017).

There are differences in pyrite contents between the two fjords that we attribute to the different forms of glacial input in each fjord. The catchments of the fjords both contain shale, coal, and other pyrite-bearing rock types (Table 1; Dallmann, 1999) and, thus, variation in bedrock lithology and sediment source does not readily explain the difference in the observed pyrite contents. However, the transport mechanism of the bedrock material to the fjords varies greatly. Van Mijenfjorden is primarily fed by extensive meltwater stream systems in Kjellströmdalen and Reindalen, while Van Keulenfjorden is fed by two tidewater glaciers, Nathorstbreen and Doktorbreen, calving directly into fjord waters (Fig. 1). Proglacial meltwater

stream material is altered through physical abrasion, oxidation of reduced sulfur, iron, and manganese, consumption of nutrients by microorganisms, and precipitation of mineral phases (Anderson et al., 2000; Wadham et al., 2001; Cooper et al., 2002). These processes, including pyrite oxidation, are also known to occur in the subglacial environment (Wadham et al., 2004) and therefore likely influence the glacial sediment delivered to both Van Mijenfjorden and Van Keulenfjorden. However, we hypothesize that transport in proglacial and riverine zones along Van Mijenfjorden introduces an additional processing step and allows further oxidation and weathering of glacial material, leading to the observed lower CRS contents in Van Mijenfjorden compared to Van Keulenfjorden sediments.

The proglacial oxidation of pyrite and other reduced iron-sulfur compounds may produce highly reactive nanoparticulate or amorphous Fe-OHO phases (Hawkings et al., 2018; Raiswell et al. 2018) and contribute to further oxidation of pyrite following deposition in the fjord sediments. Additionally, physical abrasion during transport in the meltwater stream may generate oxide and pyrite particles that are smaller in size and have greater reactive surface areas, increasing reaction rates in the fjord sediments. This hypothesis of increased pyrite/oxide reactivity following transport in proglacial streams is supported by the increases in pore water sulfate with depth at VM-In (Fig. 4a).

While in situ pyrite oxidation likely also occurs at VK-In, rapid and possibly pulse-like deposition of sediment from the glacier inhibits excess sulfate accumulation in the pore water while simultaneously refreshing the detrital pyrite supply. Thus, it is difficult to disentangle the effects of pro-glacial weathering on in situ pyrite oxidation from the effects of variable accumulation rates in the two fjords. Under the premise of constant source contributions during sedimentation (see Section 2), the overall lower CRS contents in Van Mijenfjorden (Fig. 4c, f)

do however provide evidence for the occurrence of pyrite oxidation in the meltwater streams feeding Van Mijenfjorden in contrast to the glacial systems feeding Van Keulenfjorden.

*5.3 Iron and manganese cycling*

The observed Fe and Mn pore water profiles are governed mainly by the abiotic and biotic reductive dissolution of Fe- and Mn-OHO minerals in the anoxic regions of the sediment (Lovley, 1993; Postma, 1985; Burdige and Nealson, 1986; Burdige, 1993) and the re-oxidation of mobilized $Fe^{2+}$ and $Mn^{2+}$in the oxic surface layers (Burdige, 1993; Aller, 1994). In the outer regions of both fjords, the pore water Fe gradient is closer to the sediment surface, suggesting overall more reducing conditions in the sediment compared to the inner sites where increases in pore water Fe are observed deeper in the sediment and oxygen penetration is likely deeper. These conditions in the outer regions may be caused by the greater availability of organic carbon (i.e. higher concentration of labile organic carbon per unit volume), as discussed above (Section 5.2). In these fjords, the dilution of the labile organic carbon by unreactive glacial flour closer to glacial sources appears to result in the inverse correlation of volumetric reaction rate with accumulation rate (Froelich, 1979; see Aller, 2014 and references therein). Additionally, the proximity of the Fe reduction zone to the sediment surface could be influenced by the lower overall accumulation rates in the outer regions of the fjord, which allow more time for organic matter degradation and establishment of redox gradients near the sediment surface. At VK-Out and VM-Out, decreases in the easily reducible and reducible fractions with depth align with an increase in pore water Fe concentration, suggesting that these pools are an important source of pore water Fe in the deep sediment. At the surface, mobilized $Fe^{2+}$ is re-oxidized and forms the observed solid phase surface Fe enrichments in the easily reducible and reducible fractions at the

middle and outer sites in both fjords (Fig. 5; Burdige, 1993; Aller, 1994). These surface enrichments may also include a contribution of benthically recycled Fe-OHO laterally advected from adjacent sediments (Scholz et al., 2014a, 2014b; Wehrmann et al., 2014).

At the middle and outer sites (VM-Mid, VM-Out, VK-Out), relatively constant pore water Fe concentrations at depth co-occurring with sulfate reduction suggest a balance between the rate of $Fe^{2+}$ production via biotic and abiotic Fe(III) reduction, including the reduction of Fe-OHO by hydrogen sulfide, and $Fe^{2+}$ removal by interaction with sulfide (Jørgensen and Nelson, 2004). The accumulation of AVS at these sites is evidence of the removal of Fe(II) into iron monosulfides. The abundance of reactive Fe oxides causes hydrogen sulfide and sulfur intermediate phases to be rapidly turned over at low concentration as they are shuttled between sulfate and solid metal sulfides (Wehrmann et al., 2017).

Solid and aqueous Mn data are also consistent with overall more reducing sediments at the outer sites in both fjords. Microbial Mn reduction is stimulated by the same factors that increase Fe reduction; however, the removal of Mn(II) from the pore water is controlled by Fe rather than sulfide. There are no discernable pore water Mn peaks at VM-Out and VK-Out, indicating that the Mn reduction zone and pore water peak are compressed to within the topmost 0-1 cm (Fig. 6c, f). Due to this compression, a fraction of the diagenetically mobilized Mn may escape to the water column in the outer regions of the fjord, followed by transport out of the fjord and sedimentation on the adjacent continental shelf (Shaw et al., 1990; Burdige, 1993; Thamdrup et al., 1994; März et al., 2011; Richard et al., 2013; Wehrmann et al., 2014). At the sediment surface, another fraction of the mobilized Mn(II) re-oxidizes within the sediment, forming the observed solid phase Mn enrichments in the surficial sediments at the middle and outer sites in both fjords (Fig. 6). The enrichments occur predominantly in the acid-soluble

phase. Although the acid-soluble step was designed to target Fe-carbonate minerals (Poulton and Canfield 2005), it is unlikely that the acid-soluble Mn fraction contains exclusively Mn-carbonate. The pore water in this region of the sediment is undersaturated with respect to rhodochrosite ($MnCO_3$; assuming pH ~7.5), and the measured TIC (i.e. carbonate) contents are low relative to the recovered Mn content and constant with depth (see Supplemental Figure S1); therefore, the acid-soluble Mn fraction likely contains Mn from other phases, such as a tightly bound surface-adsorbed fraction that was not desorbed during the extractable step (a magnesium chloride wash). Aqueous Mn(II) is removed from the pore water at depth at the middle and outer sites (Fig. 6), potentially due to the pool of reducible Fe present, as Mn(II) can be abiotically oxidized by Fe(III) (Burdige, 1993).

Interestingly, Fe and Mn cycling at the inner sites may be influenced by carbonate mineral (e.g. siderite, kutnahorite, and rhodochrosite) precipitation due to the high pore water carbonate and dissolved metal concentrations (Suess, 1979; Aller and Rude, 1988). Based on calculated saturation states, the pore water at VM-In is supersaturated with respect to both siderite ($FeCO_3$) below 17 cmbsf, and rhodochrosite between 7-27 cmbsf (Supplemental Table S3).

The inner site in Van Mijenfjorden experiences Fe release at ~15 cmbsf and Mn release at ~4 cmbsf, while the inner site in Van Keulenfjorden exhibits only some Mn release below ~15 cm depth, and no Fe release above ~55 cmbsf (Figs. 5 and 6). Pore water concentrations of both metals are also much higher at VM-In relative to VK-In. This may reflect the pulse-like deposition of glacial material associated with the glacier surge in Van Keulenfjorden, followed by slow re-establishment of reducing fronts. This is supported by our radionuclide data (see

Section 5.1) and by comparing the findings of Wehrmann et al. (2014), who sampled VK-In in 2011 and found dissolved Fe and Mn profiles similar to what we observe in Van Mijenfjorden.

Van Mijenfjorden has higher total extractable solid phase Fe and Mn at the inner site, relative to the inner site in Van Keulenfjorden (Figs. 5 and 6). This difference in Fe and Mn contents may be explained by the difference in meltwater stream versus tidewater glacier input in the two fjords. We propose that the additional oxidation and weathering of detrital sulfides occurring within the riverine and proglacial zone feeding Van Mijenfjorden (discussed in Section 5.2) may concentrate and transport Fe and Mn in more reactive forms to the fjord sediments (Chillrud et al., 1994; Anderson et al., 2000; Cooper et al., 2002). In Van Keulenfjorden, material entering at the head of the fjord lacks this extra processing due to direct sediment delivery via the surge-type tidewater glacier.

### *5.4 Trace element diagenesis*

The trace elements investigated in this study (As, Co, Cu, Mo, Ni, and U) are redox sensitive and/or interact with redox sensitive elements such as Fe, Mn, and S. Therefore, their behaviors in the sediment differ across the fjord axis as redox conditions and rates of dissimilatory metal and sulfate reduction change in response to increased availability of labile marine organic carbon near the fjord mouth. In the following sections, trace elements will be grouped according to the strength of their interactions with Fe and Mn cycling (Co and Ni), sulfur cycling (Cu), or both (As, Mo, and U) at the investigated sites.

#### *5.4.1. Cobalt and Nickel: Fe- and Mn-linked*

The alignment between Co, Ni, and Mn pore water peaks at all sites (Figs. 6-8) indicates that Co and Ni are tightly correlated and that both are released during reductive Mn-OHO dissolution in these fjords. Such close associations between Co, Ni, and Mn have been well-described in high latitude and other marine settings, and likely occur because Co and Ni adsorb onto or incorporate into Mn-OHO (Shaw et al., 1990; Manceau et al., 1992; Achterberg et al., 1997; Peacock and Sherman, 2007; März et al., 2011; Swanner et al., 2014; Meinhardt et al., 2016). In the fjord sediments, Co and Ni also exhibit pore water increases in zones of Fe reduction spatially separated from Mn reduction (VK-In and VK-Mid), suggesting that both Co and Ni also associate with Fe-OHO. This is particularly interesting for Co, because the relationship of Co to Fe has been less thoroughly described than the relationship of Co to Mn (Achterberg et al., 1997; Gunnarsson et al., 2000; Stockdale et al., 2010; Swanner et al., 2014). In contrast, there are many examples of the association between Ni and Fe-OHO in aquatic settings (Achterberg et al., 1997; Zegeye et al., 2012; Eickhoff et al., 2014; Robbins et al., 2016). Similar to Fe and Mn, solid phase Co and Ni are enriched in the easily reducible and reducible fractions in the surface at the outer sites in both fjords.

The behavior of Co and Ni also differs between the two fjords. Compared to Van Mijenfjorden, Van Keulenfjorden has higher Co and Ni contents in the oxidizable and exchangeable fractions, along with generally higher Ni and Co pore water concentrations (Figs. 7 and 8). The oxidizable step of the extraction likely targeted a significant fraction of pyrite (up to ~40%), which typically contains substantial amounts of Co and Ni incorporated in the mineral (Morse and Luther III, 1999; Stockdale et al., 2010; Gregory et al., 2015). Thus, the elevated values of oxidizable Co and Ni found in Van Keulenfjorden sediments are likely related to the higher pyrite contents in the Van Keulenfjorden sediments (Fig. 4) due to direct delivery from

the tidewater glacier. In Van Keulenfjorden, the exchangeable fraction accounts for 6% and 7% of the total extractable quantity of Co and Ni respectively, while in Van Mijenfjorden the exchangeable fraction accounts for 4% of both Co and Ni. This difference, though small, may indicate that the crystalline Fe and Mn oxides delivered by the tidewater glacier hold more adsorbed Co and Ni than those that are processed in the Van Mijenfjorden meltwater stream system prior to entering the fjord. Overall it seems that due to the delivery of large amounts of Fe- and Mn-OHO directly from the tidewater glacier, without additional processing in the proglacial zone, there is more early diagenetic cycling of Co and Ni in Van Keulenfjorden than in Van Mijenfjorden, especially at VK-Mid and VK-Out where the pore water concentrations are higher and the surface solid phase enrichment is larger relative to VM-Mid and VM-Out.

*5.4.2. Copper: Sulfur linked*

The head-to-mouth fjord trend of decreasing pore water Cu concentrations (Fig. 9) is likely related to higher sulfate reduction rates at the middle and outer sites. In anoxic, sulfate reducing environments, Cu(II) is reduced by sulfide to Cu(I), subsequently precipitates in sulfide minerals (Calvert and Pedersen, 1993; Öztürk, 1995; Zaggia and Zonta, 1997; Morse and Luther III, 1999), and can form a large variety of Cu sulfide minerals at a lower sulfide concentration than is required to form Fe-sulfide minerals (Pattrick et al., 1997; Morse and Luther III, 1999). Therefore, Cu is more readily removed from the pore water at increasing distances from the glacial input, where sulfate reduction rates are higher. The presence of Cu in the pore water at VM-Mid seems to counter this trend, but may be due to a separate process related to solid phase sulfides, as described below.

The scatter in pore water Cu concentrations is unlikely to be caused by the proximity of the measured concentration to the detection limit, because other elements with similar detection limits such as Ni (with a detection limit of 0.16 nM; Supplemental Table S2) were measured in the same concentration ranges (up to 0.5 μM) and do not show the same degree of scatter. This scatter may instead be related to a heterogeneous distribution of dissolved Cu sources and sinks such as sulfide minerals and recalcitrant organic matter (Shaw et al., 1990; Widerlund, 1996; Skrabal et al., 2000; Caetano et al., 2003; Audry et al., 2006). Thus, the turnover time, τ, of aqueous Cu is faster than the rate of diffusional exchange between our sampled depth intervals (2-4 cm), which can be calculated (based on a porosity of 0.75 and a Cu diffusion coefficient of $3.2 \times 10^{-6}$ $cm^2$ $s^{-1}$ and transport scales of 2-4 cm) to be τ~20 days (Iversen and Jørgensen, 1993; Jørgensen, 1993; Schulz and Zabel, 2006).

Copper may be delivered to the sediment in association with both Fe- and Mn-OHO (Fig. 9; Fernex et al., 1992; Peacock and Sherman, 2004; Sherman and Peacock, 2010). However, given that the majority of the solid phase Cu is in the acid-soluble fraction (Fig. 9), it is likely that Cu primarily associates with Mn-OHO (Sherman and Peacock 2010; Little et al., 2015), as the acid-soluble fraction also contains the highest Mn contents (Fig. 6).

At the middle and outer sites in both fjords, solid phase Cu decreases below the surface 2-4 cm as it is transferred, through a transient pore water reservoir not detectable with our sampling methods, to another solid phase pool that was not targeted in our extraction. Cu-S minerals such as covellite (CuS) and chalcocite ($Cu_2S$) are poorly soluble in HCl-based extractions, and chalcocite in particular is generally leached using sulfuric acid-based techniques (Cheng and Lawson, 1991; Cooper and Morse, 1998). Small increases in oxidizable Cu at depth indicate that some Cu is removed to pyrite or other Cu-S minerals that were dissolved in the oxidizable step.

At the inner sites, this depletion does not occur due to low sulfate reduction rates and lack of sulfide mineral formation, and therefore solid phase Cu contents remain high at depth.

Higher pore water Cu concentrations at VM-Mid relative to VK-Mid may reflect the influence of oxidizing detrital pyrites, which likely either contain Cu inclusions or co-occur with Cu-sulfide minerals (Huerta-Diaz and Morse, 1992; Sun and Püttmann, 2000; Gregory et al., 2015). Higher aqueous Cu concentrations due to an additional source from detrital pyrites would support our hypothesis of greater delivery of partially oxidized and more reactive sulfide minerals in meltwater stream sediments in Van Mijenfjorden.

*5.4.3 Uranium, Molybdenum, and Arsenic: Fe-Mn-S linked*

The removal of U from the pore water at all sites (except VK-In, discussed below) is likely due to reduction following entry into the sediment. In the water column, U is generally stable and conservative in dissolved uranyl (U(VI)) carbonate complexes, and thus primarily enters the sediment through diffusion across the sediment-water interface (Ku et al., 1977; Anderson, 1987). At VM-In, we observe a gradual removal from the pore water within the zone of pore water Fe release, but no coincident increase in solid phase U, possibly due to dilution of authigenic solid U phases by the high accumulation rate observed at this site (Fig. 10a). In the outer regions of the fjord, however, U is removed from the pore water closer to the sediment surface, and accumulates in the solid phase, as reflected in the elevated solid contents at these sites (Fig 10b-c, e-f). The reduction of U is tightly coupled to both Fe and sulfate reduction in anoxic sediment, and following reduction to U(IV) it adsorbs to particle surfaces or precipitates, possibly as uraninite or meta-stable uraninite precursors (Anderson, 1987; McKee et al., 1987; Klinkhammer and Palmer, 1991; Barnes and Cochran, 1993; Zheng et al., 2002; Morford et al.,

2009). The observed solid phase U content increases are primarily in the exchangeable fraction, suggesting that the primary mode of pore water U removal is adsorption of U(IV) to particle surfaces. Fe- and sulfate-reducing organisms are capable of directly reducing U, potentially as a terminal electron acceptor (Cochran et al., 1986; Lovley et al., 1991; Lovley and Phillips, 1992). We conclude that at VM-In, U is likely reduced predominantly by Fe-reducing organisms (Lovley et al., 1991) while in the outer regions of both fjords, the combined activity of sulfate and Fe reducing bacteria make the sediments a more efficient sink for pore water U, which adsorbs to particle surfaces following reduction at depth (Lovley and Phillips, 1992; Gu et al., 2005). At VK-In, the only site where U increases in the pore water, high pore water carbonate concentrations (Supplemental Table S3) may cause U to desorb from Fe-OHO and form soluble uranyl carbonate complexes (Allard, 1982; Gu et al., 2005). In contrast, VM-In contains notably less U in the exchangeable fraction, which could be the result of the oxidation and stripping of U from particle surfaces during transport in meltwater streams.

Diagenetic alteration of Mo-phases is affected by both Fe and sulfate reduction, with Mn reduction playing a smaller role (Fig. 11). Typically, Mo is assumed to associate more with Mn-OHO (Bertine and Turekian, 1973; Shimmield and Price, 1986; Shaw et al., 1990; Crusius et al., 1996; März et al., 2011; Meinhardt et al., 2016), and the interaction between Mo and Fe in modern marine sediments has been less thoroughly established (Arnold et al., 2004; Poulson et al., 2006). The Mo-Fe interaction in the Svalbard fjords is most apparent at VK-In, VK-Mid, and VM-In, where there is spatial separation between the zones of Fe and Mn reduction (Fig. 11). The removal of Mo from the pore water in the Mn reduction zone most likely occurs when $Fe^{2+}$ is oxidized by Mn(IV) and precipitates (Burdige, 1993; Postma and Appelo, 2000), causing pore water Mo to adsorb to the fresh Fe-OHO surfaces (Gustafsson, 2003; Goldberg et al., 2009). Any

Mo that is released from the dissolving Mn-OHO in this process may immediately re-adsorb to the Fe-OHO. Upon burial deeper into the Fe reduction zone, Mo is released back into the pore water as Mo-rich Fe-OHO dissolves (Fig. 11a, e). At VK-Out, VM-Mid, and VM-Out, surface solid phase Mo enrichments in the easily reducible and reducible fractions lie directly above pore water maxima in the sediment column (Fig. 11), which suggests that the precipitation of fresh Mn- and Fe-OHO at the oxic sediment surface serves as a sink for dissolved Mo released at depth. The same process may occur at VK-Out even though our sampling resolution did not capture the sediment surface pore water depletion.

The removal of pore water Mo in the deeper sediment layers at VK-Out, VM-Mid, and VM-Out (Fig. 11) is most likely due to the reduction of Mo(VI), followed by precipitation and/or adsorption to particle surfaces. Mo becomes particle reactive at a certain sulfide concentration threshold (Helz et al., 1996; Zheng et al., 2000). Given the relatively high proportion of solid phase Mo in the exchangeable fraction in the deepest samples (Fig. 11), the adsorption of reduced Mo may be of particular importance. Interestingly, removal occurs at VK-In, VK-Out, VM-Mid, and VM-Out despite the absence of detectable $H_2S$ at depth, suggesting that at these locations either it is not necessary for sulfide concentrations to be above the sulfide concentration threshold for Mo sulfidization to occur, or the reduction and removal is accomplished through direct interaction with sulfate reducing bacteria rather than indirectly through pore water sulfide (Helz et al., 1996; Tucker et al., 1997; Zheng et al., 2000).

Arsenic is released to the pore water within the zone of Fe oxide dissolution (Fig. 12), demonstrating a strong linkage between As and Fe cycling which can be explained by As adsorption onto and co-precipitation with Fe-OHO as previously observed in high latitude sediments and many other settings (Aggett and O'Brien, 1985; Brannon and Patrick, 1987;

Cullen and Reimer, 1989; Belzile and Tessier, 1990; März et al., 2011; Burton et al., 2013; Meinhardt et al., 2016). The large proportions of solid phase As in the reducible fraction (Fig. 12) suggest that solid phase As is primarily associated with crystalline Fe-OHO. However, pore water As behavior does not perfectly mirror Fe trends in the fjords (Fig. 12). For example, overall pore water As concentrations at depth increase with distance from the glacier in both fjords, a trend that is not reflected in the Fe profiles (Fig. 5). Instead, these pore water As increases appear to be controlled by factors other than the reductive dissolution of Fe(III), and particularly correlate with higher sulfate reduction rates, suggesting that microbial sulfate reduction may trigger the release of dissolved As from the solid phase (Keimowitz et al., 2007). Burton et al. (2013) found that anoxic sediment columns amended with As(III) released more dissolved As when they had been inoculated with sulfate reducing bacteria as compared to sterilized columns. This may be explained by a ligand exchange at the surface of Fe oxides, such as goethite, that leads to the replacement of adsorbed As with the sulfide produced during microbial sulfate reduction (Burton et al., 2013). The reduction of Fe(III) by sulfide leads to the formation of FeS (mackinawite), which does not adsorb or incorporate As (Kirk et al., 2010). Our data indicate that this process occurs in the middle and outer sites of both fjords, where the alteration of Fe oxides that are coated with and eventually replaced by mackinawite (Kocar et al., 2010; Burton et al., 2011, 2013) leads to the release of dissolved As into the pore water. This is supported by the co-occurrence of elevated AVS contents (Fig. 4b, e) and high dissolved As concentrations (Fig. 12b-c, e-f). Further, As is released to the pore water in the same area where Mo is removed at VM-Mid (below 47 cmbsf), VM-Out (below 3 cm), and VK-Out (below 2.5 cm) (Fig. 11b-c, f and Fig. 12b-c, f). This could indicate an increase in the availability of sulfide, which simultaneously mobilizes As and removes dissolved Mo (Helz et al., 1996; Burton et al.,

2013). In contrast, the inner sites in both fjords have the lowest sulfate reduction rates and therefore the As released during Fe reduction at these sites may be rapidly re-adsorbed to oxide particles rather than accumulating in the pore water. Additionally, the glacial sediment source at the inner sites may supply large amounts of freshly ground, Fe-OHO-rich particles with vacant adsorption sites that serve as efficient sinks for the released As.

## *6. Summary and conclusions*

### *6.1 Biogeochemical gradients along the head-to-mouth fjord axis*

This investigation reveals landscape-scale biogeochemical gradients in Van Mijenfjorden and Van Keulenfjorden from the glacially influenced fjord head to the marine influenced mouth (Fig. 13b). Sediment accumulation rate near the glacial input is high and, based on previous research, likely decreases toward the mouth of the fjord. Unlike open marine systems, sedimentation and labile organic carbon flux are decoupled in these fjords. Close to the glacial source, dilution of labile organic carbon by high accumulation of metal oxide-rich glacial flour may suppress microbial reduction rates and promote benthic oxidation of detrital pyrite. In the outer fjord regions with lower accumulation of glacial flour, greater availability of labile, marine organic carbon likely contributes to the observed higher net sulfate reduction rates and accumulation of sulfide minerals, along with the compression of Fe and Mn reduction zones near the sediment surface. This generates authigenic Fe- and Mn-OHO enrichments in the surface sediments of the outer fjord, and may increase the potential for transport of Fe and Mn into the water column through diffusion across the sediment-water interface or resuspension of enriched surface sediments.

Journal Pre-proofs

All trace elements investigated in this study are influenced by Fe, Mn, and sulfur cycling (Fig. 13c); however, the strength of the interaction with these cycles is different for each element and their diagenetic behaviors are controlled by the head-to-mouth gradients in the availability of labile organic carbon as described above. Cobalt and nickel are closely coupled to Fe and Mn cycling, and show similar release into the pore water with oxide reduction at depth coupled with re-oxidation and solid phase enrichment at the sediment surface, particularly at the outer sites. In contrast, copper appears to be predominantly controlled by sulfur transformations, with release into the pore water during sulfide oxidation near the head of the fjord and precipitation in authigenic sulfide minerals in the outer regions where higher sulfate reduction rates occur. Uranium is reduced and scavenged from the pore water in association with Fe and sulfate reduction, so the sediments become a more efficient sink for dissolved uranium with increasing distance from the glacier. Molybdenum behavior is controlled by Fe cycling close to the glacier, but is likely reduced and removed from the pore water with increasing sulfate reduction rates out-fjord. Arsenic is linked with Fe cycling at the inner fjord sites, but becomes de-coupled as Fe particles become coated with Fe-monosulfides at the outer sites, driving accumulation of As in the pore water.

*6.2 Comparison between tidewater glacier- and meltwater stream-dominated sediment delivery*

The two fjords in this study share similar catchment area bedrock lithologies, water column circulation, and organic matter delivery to the sediments. Thus, the subtle differences between the fjords may be attributable to differences in the supplies of glacial sediment from the surging tidewater glacier in Van Keulenfjorden and the extensive meltwater stream systems in Van Mijenfjorden (see Fig. 13a). The largest differences are in the inner regions of the fjords,

where glacial impact and source processing are highest. The sediment accumulation rate at the inner site in VM is lower than the estimated minimum rate at the inner site in VK, most likely due to a combination of sediment trapping in the meltwater streams feeding VM and an increase in sediment delivery associated with the recent surge of Nathorstbreen in VK. The sediments at the inner regions of VK have large contents of pyrite, likely detrital and eroded from the underlying bedrock, and the trace element cycling appears limited, potentially by rapid deposition of crystalline, less reactive glacial flour during the recent tidewater glacier surge. In contrast, the inner site in VM shows evidence of strong trace element cycling and contains comparatively less pyrite. We suggest that proglacial and riverine processing in the Van Mijenfjorden meltwater streams allows for additional transformation of material from glacial discharge by oxidizing detrital sulfide minerals and generating more reactive particulate trace element species through physical, chemical, and biological weathering.

At the inner and middle sites of VM, zones of Fe and Mn reduction and associated aqueous Co, Ni, and As release are closer to the sediment surface relative to the corresponding sites in VK, possibly due to a lower accumulation rate and a higher content of total extractable (i.e. reactive) trace metal phases. The inner and middle sites in VM contain higher pore water concentrations of Cu, which could be caused by in situ oxidation of Cu-bearing sulfide minerals. Solid U content at VM-In is lower than at VK-In and there is net removal from the pore water, potentially the result of the stripping of adsorbed U from particle surfaces during transport in the meltwater streams feeding VM followed by re-adsorption onto particle surfaces within the sediment. Solid phase Mo is enriched in VM-In relative to VK-In, and a greater release to the pore water is observed within the Fe reduction zone.

Journal Pre-proofs

*6.3 Impact of glacial retreat on trace element cycling*

Glaciers are currently experiencing net mass loss due to climate change (Dowdeswell et al., 1997). As a result, many tidewater glaciers are retreating into subaerial valleys (Ziaja, 2001). This study demonstrates that a change from tidewater glacier to meltwater stream sediment supply may have an impact on trace element processing in coastal sediments. However, it is important to note that the findings of this study cannot be extrapolated to all other fjords, where different conditions such as circulation and bedrock composition may exert different controls on trace element cycling in the sediments.

With glacial retreat, glaciated fjord systems similar to those in this study may experience greater weathering during sediment transport in meltwater streams, reducing the delivery of detrital minerals (e.g. pyrite) to the fjord and transferring associated trace elements into more reactive phases (e.g. amorphous oxides). This delivery of more reactive trace metal phases along with lower sediment accumulation rates may drive zones of Fe and Mn reduction closer to the sediment surface and allow accumulation of reduced metals in the pore water in the regions close to the glacial input. Thus, the retreat of tidewater glaciers may drive increased benthic cycling and possible remobilization of Fe, Mn, Co, Ni, Mo, and As from reactive oxides and of Cu from weathered sulfide minerals. In contrast, the sediments may become a more efficient sink for elements such as U that are stripped from particle surfaces during stream transport and re-adsorbed in reducing sediment. Overall, these shifts in trace element diagenetic behavior and potential transport with glacial retreat could impact the biogeochemical cycling of carbon and nutrients along glaciated coastlines and within polar oceans.

*Acknowledgements*

We thank the captain (Stig Henningsen) and first mate (Reidar Sørensen) aboard MS *Farm* for their assistance during the 2016 sampling campaign. We thank the staff of the Kings Bay Marine Laboratory and the AWIPEV Arctic Research Base in Ny Ålesund for their assistance and provision of lab space. We are indebted to Susann Henkel and Sabine Kasten of the Alfred Wegener Institute for their support of the research expedition and the scientific party of the 2016 campaign for their assistance, stimulating discussions, and good company. Many thanks to: Katie Wooton and Troy Rasbury of the FIRST@Stony Brook, who provided technical assistance and the use of their mass spectrometer for trace element analysis; Isaac Klingensmith, who provided lab assistance and advice; and Julia Stepanuk, who provided essential help with ArcGIS and R Studio for the making of the map and figures in this paper. Geospatial imagery and support was provided by the Polar Geospatial Center and Brad Herried, under NSF-OPP awards 1043681 & 1559691. This research was funded by a Minghua Zhang Early Career Faculty Innovation Award to LMW at SoMAS, SBU-SUNY and partially supported by postdoctoral fellowships from the US-National Science Foundation [EAR-PF1625158 to ABM], and German Research Foundation [DFG 389371177 to KL]. Access to the AWIPEV Arctic Research Base in Ny Ålesund was granted by the AWI under project nr. KOP 56 (RiS #10528). We also thank the editor of this paper, C. Peacock, and acknowledge the insightful reviews provided by C. März and two anonymous reviewers.

*References*

Achterberg E.P., van den Berg C.M.G., Boussemart M., Davison W. (1997) Speciation and cycling of trace metals in Esthwaite Water: A productive English lake with seasonl deep-water anoxia. *Geochim. Cosmochim. Acta* **61**, 5233–5253. https://doi.org/10.1038/nature19355.Hiess

Aggett J., O'Brien G.A. (1985) Detailed model for the mobility of arsenic in lacustrine sediments based on measurements in Lake Ohakuri. *Environ. Sci. Technol*. **19**, 231–238.

Algeo T.J., Maynard J.B. (2004) Trace-element behavior and redox facies in core shales of Upper Pennsylvanian Kansas-type cyclothems. *Chem. Geol*. **206**, 289–318. https://doi.org/10.1016/j.chemgeo.2003.12.009

Algeo T.J., Rowe H. (2012) Paleoceanographic applications of trace-metal concentration data. *Chem. Geol*. **324–325**, 6–18. https://doi.org/10.1016/j.chemgeo.2011.09.002

Allard B. (1982) Solubilities of actinides in neutral or basic solutions. *Actinides Perspect*. 553–580.

Aller R.C. (1994) The sedimentary Mn cycle in Long Island Sound: Its role as intermediate oxidant and the influence of bioturbation, O2, and Corg flux on diagenetic reaction balances. *J. Mar. Res*. **52**, 259–295. https://doi.org/10.1357/0022240943077091

Aller R.C., Rude P.D. (1988) Complete oxidation of solid phase sulfides by manganese and bacteria in anoxic marine sediments. *Geochim. Cosmochim. Acta* **52**, 751–765.

Anderson R.F. (1987) Redox behavior of uranium in an anoxic marine basin. *Uranium* **3**, 145–164.

Anderson S.P., Drever J.I., Frost C.D., Holden P. (2000) Chemical weathering in the foreland of a retreating glacier. *Geochim. Cosmochim. Acta* **64**, 1173–1189. https://doi.org/10.1016/S0016-7037(99)00358-0

Anderson S.P., Drever J.I., Humphrey N.F. (1997) Chemical weathering in glacial environments. *Geology* **25**, 399-402. https://doi.org/10.1130/00917613(1997)025<0399:CWIGE>2.3.CO;2

Appleby P.G., Oldfield F. (1978) The calculation of lead-210 dates assuming a constant rate of supply of unsupported 210Pb to the sediment. *Catena* **5**, 1–8. https://doi.org/10.1016/S0341-8162(78)80002-2

Arnold G.L., Anbar A.D., Barling J., Lyons T.W. (2004) Molybdenum isotope evidence for widespread anoxia in mid-Proterozoic Oceans. *Science* **304**, 87–90. https://doi.org/10.1029/2002GC000356

Arnosti C., Jørgensen B.B. (2006) Organic carbon degradation in Arctic marine sediments, Svalbard: A comparison of initial and terminal steps. *Geomicrobiol. J*. **23**, 551–563. https://doi.org/10.1080/01490450600897336

Audry S., Blanc G., Schäfer J., Chaillou G., Robert S. (2006) Early diagenesis of trace metals (Cd, Cu, Co, Ni, U, Mo, and V) in the freshwater reaches of a macrotidal estuary. *Geochim. Cosmochim. Acta* **70**, 2264–2282. https://doi.org/10.1016/j.gca.2006.02.001

Barnes C.E., Cochran K.J. (1993) Uranium geochemistry in estuarine sediments: Controls on removal and release processes. *Geochim. Cosmochim. Acta* **57**, 555–569.

Belzile N., Tessier A. (1990) Interactions between arsenic and iron oxyhydroxides in lacustrine sediments. *Geochim. Cosmochim. Acta* **54**, 103–109. https://doi.org/10.1016/0016-7037(90)90198-T

Bertine K.K., Turekian K.K. (1973) Molybdenum in marine deposits. *Geochim. Cosmochim. Acta* **37**, 1415–1434. https://doi.org/10.1016/0016-7037(73)90080-X

Bhatia M.P., Kujawinski E.B., Das S.B., Breier C.F., Henderson P.B., Charette M.A. (2013) Greenland meltwater as a significant and potentially bioavailable source of iron to the ocean. *Nat. Geosci*. **6**, 274–278. https://doi.org/10.1038/ngeo1746

Bliss A., Hock R. and Radić V. (2014) Global response of glacier runoff to twenty-first century climate change. *J. Geophys. Res. Earth Surf.* **119**, 717–730.

Bottrell S.H., Tranter M. (2002) Sulphide oxidation under partially anoxic conditions at the bed of the Haut Glacier d'Arolla, Switzerland. *Hydrol. Process*. **16**, 2363–2368. https://doi.org/10.1002/hyp.1012

Buongiorno J., Herbert L. C., Wehrmann L. M., Michaud A. B., Laufer K., Røy H., Jørgensen B. B., Szynkiewicz A., Faiia A., Yeager K. M., Schindler K. and Lloyd K. G. (2019) Complex microbial communities drive iron and sulfur cycling in Arctic fjord sediments. *Appl. Environ. Microbiol.* **85**, e00949-19.

Bourgeois S., Kerhervé P., Calleja M.L., Many G., Morata N. (2016) Glacier inputs influence organic matter composition and prokaryotic distribution in a high Arctic fjord (Kongsfjorden, Svalbard). *J. Mar. Syst*. **164**, 112–127. https://doi.org/10.1016/J.JMARSYS.2016.08.009

Boyd E.S., Hamilton T.L., Havig J.R., Skidmore M.L., Shock E.L. (2014) Chemolithotrophic primary production in a subglacial ecosystem. *Appl. Environ. Microbiol*. **80**, 6146–6153. https://doi.org/10.1128/AEM.01956-14

Brannon J.M., Patrick W.H. (1987) Fixation, transformation, and mobilization of arsenic in sediments. *Environ. Sci. Technol*. **21**, 450–459.

Brüchert V., Knoblauch C., Jørgensen B.B. (2001) Controls on stable sulfur isotope fractionation during bacterial sulfate reduction in Arctic sediments. *Geochim. Cosmochim. Acta* **65**, 763–776. https://doi.org/10.1016/S0016-7037(00)00557-3

Brumsack H.J. (2006) The trace metal content of recent organic carbon-rich sediments: Implications for Cretaceous black shale formation. *Palaeogeogr. Palaeoclimatol. Palaeoecol*. **232**, 344–361. https://doi.org/10.1016/j.palaeo.2005.05.011

Burdige D.J. (1993) The biogeochemistry of manganese and iron reduction in marine sediments. *Earth Sci. Rev*. **35**, 249–284. https://doi.org/10.1016/0012-8252(93)90040-E

Burdige D.J., Nealson K.H. (1986) Chemical and microbiological studies of sulfide - mediated manganese reduction. *Geomicrobiol. J*. **4**, 361–387.

Burton E.D., Johnston S.G., Bush R.T. (2011) Microbial sulfidogenesis in ferrihydrite-rich environments: Effects on iron mineralogy and arsenic mobility. *Geochim. Cosmochim. Acta* **75**, 3072–3087. https://doi.org/10.1016/j.gca.2011.03.001

Burton E.D., Johnston S.G., Planer-Friedrich B. (2013) Coupling of arsenic mobility to sulfur transformations during microbial sulfate reduction in the presence and absence of humic acid. *Chem. Geol*. **343**, 12–24. https://doi.org/10.1016/J.CHEMGEO.2013.02.005

Caetano M., Madureira M.-J., Vale C. (2003) Metal remobilisation during resuspension of anoxic contaminated sediment: Short-term laboratory study. *Water. Air. Soil Pollut*. **143**, 23–40. https://doi.org/10.1023/A:1022877120813

Calvert S.E., Pedersen T. (1993) Geochemistry of Recent oxic and anoxic marine sediments: Implications for the geological record. *Mar. Geol*. **113**, 67–88. https://doi.org/10.1016/0025-3227(93)90150-T

Calvert S.E., Price N.B. (1977) Geochemical variation in ferromanganese nodules and associated sediments from the Pacific Ocean. *Mar. Chem*. **5**, 43–74. https://doi.org/10.1016/0304-4203(77)90014-7

Canfield D.E. (1989) Reactive iron in marine sediments. *Geochim. Cosmochim. Acta* **53**, 619–632.

Canion A., Overholt W.A., Kostka J.E., Huettel M., Lavik G., Kuypers M.M.M. (2014) Temperature response of denitrification and anaerobic ammonium oxidation rates and microbial community structure in Arctic fjord sediments. *Environ. Microbiol*. **16**, 3331–3344. https://doi.org/10.1111/1462-2920.12593

Cappuyns V., Swennen R. and Niclaes M. (2007) Application of the BCR sequential extraction scheme to dredged pond sediments contaminated by Pb-Zn mining: A combined geochemical and mineralogical approach. *J. Geochemical Explor.* **93**, 78–90.

Charette M.A., Lam P.J., Lohan M.C., Kwon E.Y., Hatje V., Jeandel C., Shiller A.M., Cutter G.A., Thomas A., Boyd P.W., Homoky W.B., Milne A., Thomas H., Andersson P.S., Porcelli D., Tanaka T., Geibert W., Dehairs F., Garcia-Orellana J. (2016) Coastal ocean and shelf-sea biogeochemical cycling of trace elements and isotopes: lessons learned from GEOTRACES. *Philos. Trans. R. Soc. A*. **374**, 20160076. https://doi.org/10.1098/rsta.2016.0076

Chillrud S.N., Pedrozo F.L., Temporetti P.F., Planas H.F., Froelich P.N. (1994) Chemical weathering of phosphate and germanium in glacial meltwater streams: Effects of subglacial pyrite oxidation. *Limnol. Oceanogr.* **39**, 1130–1140. https://doi.org/10.4319/lo.1994.39.5.1130

Cheng C.Y., Lawson F. (1991) The kinetics of leaching chalcocite in acidic oxygenated sulphate-chloride solutions. *Hydrometallurgy* **27**, 249–268. https://doi.org/10.1016/0304-386X(91)90053-O

Cid A.P., Nakatsuka S., Sohrin Y. (2012) Stoichiometry among bioactive trace metals in the Chukchi and Beaufort Seas. *J. Oceanogr*. **68**, 985–1001. https://doi.org/10.1007/s10872-012-0150-8

Cline J.D. (1969) Spectrophotometric determination of hydrogen sulfide in natural waters. *Limnol. Oceanogr*. **14**, 454–458. https://doi.org/10.4319/lo.1969.14.3.0454

Cochran K.J., Carey A.E., Sholkovitz E.R., Surprenant L.D. (1986) The geochemistry of uranium and thorium in coastal marine seidments and sediment pore waters. *Geochim. Cosmochim. Acta* **50**, 663–680.

Cokelet E.D., Tervalon N., Bellingham J.G. (2008) Hydrography of the West Spitsbergen Current, Svalbard Branch: Autumn 2001. *J. Geophys. Res. Ocean*. **113**, C01006. https://doi.org/10.1029/2007JC004150

Cooper R.J., Wadham J.L., Tranter M., Hodgkins R., Peters N.E. (2002) Groundwater hydrochemistry in the active layer of the proglacial zone, Finsterwalderbreen, Svalbard. *J. Hydrol*. **269**, 208–223. https://doi.org/10.1016/S0022-1694(02)00279-2

Cooper D.C., Morse J.W. (1998) Extractability of metal sulfide minerals in acidic solutions: Application to environmental studies of trace metal contamination within anoxic sediments. *Environ. Sci. Technol*. **32**, 1076–1078. https://doi.org/10.1021/es970415t

Cottier F., Tverberg V., Inall M., Svendsen H., Nilsen F., Griffiths C. (2005) Water mass modification in an Arctic fjord through cross-shelf exchange: The seasonal hydrography of Kongsfjorden, Svalbard. *J. Geophys. Res. Ocean*. **110**, C12005. https://doi.org/10.1029/2004JC002757

Crusius J., Anderson R.F. (1995) Evaluating the mobility of 137Cs, 239+240Pu, and 210Pb from their distributions in laminated lake sediments. *J. Paleolimnol*. **13**, 119–141.

Crusius J., Calvert S., Pedersen T., Sage D. (1996) Rhenium and molybdenum enrichments in sediments as indicators of oxic, suboxic and sulfidic conditions of deposition. *Earth Planet. Sci. Lett*. **145**, 65–78. https://doi.org/10.1016/S0012-821X(96)00204-X

Cui X., Bianchi T.S., Savage C., Smith R.W. (2016) Organic carbon burial in fjords: Terrestrial versus marine inputs. *Earth Planet. Sci. Lett*. **451**, 41–50. https://doi.org/10.1016/J.EPSL.2016.07.003

Cullen J.T. (2006) On the nonlinear relationship between dissolved cadmium and phosphate in

the modern global ocean: Could chronic iron limitation of phytoplankton growth cause the kink? *Limnol. Oceanogr*. **51**, 1369–1380.
Cullen W.R., Reimer K.J. (1989) Arsenic Speciation in the Environment. *Chem. Rev* **89**, 713–764.
Dallmann, W. K. (Ed.) (1999) *Lithostratigraphic Lexicon of Svalbard*. Norsk Polarinstitutt, Tromsø. pp. 318.
Dickens G.R., Koelling M., Smith D.C., Schnieders L. (2007) Rhizon sampling of pore waters on scientific drilling expeditions: An example from the IODP expedition 302, Arctic Coring Expedition (ACEX), *Scientific Drilling* **4**, 22-25. https://doi.org/10.2204/iodp.sd.4.08.2007
Dowdeswell J.A., Hagen J.O., Björnsson H., Glazovsky A.F., Harrison W.D., Holmlund P., Jania J., Koerner R.M., Lefauconnier B., Simon C., Ommanney L., Thomas R.H. (1997) The mass balance of circum-Arctic glaciers and recent climate change. *Quat. Res*. **48**, QR971900.
Eickhoff M., Obst M., Schröder C., Hitchcock A.P., Tyliszczak T., Martinez R.E., Robbins L.J., Konhauser K.O., Kappler A. (2014) Nickel partitioning in biogenic and abiogenic ferrihydrite: The influence of silica and implications for ancient environments. *Geochim. Cosmochim. Acta* **140**, 65–79. https://doi.org/10.1016/j.gca.2014.05.021
Farnsworth W.R., Ingólfsson Ó., Noormets R., Allaart L., Alexanderson H., Henriksen M., Schomacker A. (2017) Dynamic Holocene glacial history of St. Jonsfjorden, Svalbard. *Boreas* **46**, 585–603. https://doi.org/10.1111/bor.12269
Fernex F., Février G., Bénaïm J., Arnoux A. (1992) Copper, lead and zinc trapping in Mediterranean deep-sea sediments: probable coprecipitation with Mn and Fe. *Chem. Geol*. **98**, 293–306. https://doi.org/10.1016/0009-2541(92)90190-G
Forwick M., Baeten N.J., Vorren T.O. (2009) Pockmarks in Spitsbergen fjords. *Nor. Geol. Tidsskr*. **89**, 65–77. https://doi.org/10.1097/PEC.0b013e31827e647f
Fossing H., Jørgensen B.B. (1989) Measurement of bacterial sulfate reduction in sediments : Evaluation of a single-step chromium reduction method. *Biogeochemistry* **8**, 205–222.
Gilbert R., Nielsen N., Mo H., Desloges J.R., Rasch M. (2002) Glacimarine sedimentation in Kangerdluk (Disko Fjord), West Greenland, in response to a surging glacier. *Mar. Geol*. **191**, 1–18.
Gleyzes C., Tellier S., Astruc M. (2002) Fractionation studies of trace elements in contaminated soils and sediments: a review of sequential extraction procedures. *Trends Anal. Chem*. **21**, 451–467.
Glud R.N., Holby O., Hoffmann F., Canfield D.E. (1998) Benthic mineralization and exchange in Arctic sediments (Svalbard, Norway). *Mar. Ecol. Prog. Ser.* **173**, 237–251.
Goldberg T., Archer C., Vance D., Poulton S.W. (2009) Mo isotope fractionation during adsorption to Fe (oxyhydr)oxides. *Geochim. Cosmochim. Acta* **73**, 6502–6516. https://doi.org/10.1016/j.gca.2009.08.004
Gregory D.D., Large R.R., Halpin J.A., Baturina E.L., Lyons T.W., Wu S., Danyushevsky L., Sack P.J., Chappaz A., Maslennikov V.V., Bull S.W. (2015) Trace element content of sedimentary pyrite in black shales. *Econ. Geol*. **110**, 1389–1410. https://doi.org/10.2113/econgeo.110.6.1389
Gu B., Wu W.-M., Ginder-Vogel M.A., Yan H., Fields M.W., Zhou J., Fendorf S., Criddle C.S., Jardine P.M. (2005) Bioreduction of uranium in a contaminated soil column. *Environ. Sci. Technol*. **39**, 4841–4847. https://doi.org/10.1021/ES050011Y
Gunnarsson M., Jakobsson A.M., Ekberg S., Albinsson Y., Ahlberg E. (2000) Sorption studies of

cobalt(II) on colloidal hematite using potentiometry and radioactive tracer technique. *J. Colloid Interface Sci*. **231**, 326-336. https://doi.org/10.1006/jcis.2000.7149

Gustafsson J.P. (2003) Modelling molybdate and tungstate adsorption to ferrihydrite. *Chem. Geol*. **200**, 105–115. https://doi.org/10.1016/S0009-2541(03)00161-X

Hall P.O.J., Aller R.C. (1992) Rapid, small- volume, flow injection analysis for SCO2, and NH4+ in marine and freshwaters. *Limnol. Oceanogr*. **37**, 1113–1119. https://doi.org/10.4319/lo.1992.37.5.1113

Harrold Z.R., Skidmore M.L., Hamilton T.L., Desch L., Amada K., Van Gelder W., Glover K., Roden E.E., Boyd E.S. (2016) Aerobic and anaerobic thiosulfate oxidation by a cold-adapted, subglacial chemoautotroph. *Appl. Environ. Microbiol*. **82**, 1486–1495. https://doi.org/10.1128/AEM.03398-15

Hawkings J. R., Wadham J. L., Tranter M., Raiswell R., Benning L. G., Statham P. J., Tedstone A., Nienow P., Lee K., Telling J. (2014) Ice sheets as a significant source of highly reactive nanoparticulate iron to the oceans. *Nat. Commun.* **5**, 3929.

Hawkings J.R., Benning L.G., Raiswell R., Kaulich B., Araki T., Abyaneh M., Stockdale A., Koch-Müller M., Wadham J.L., Tranter M. (2018) Biolabile ferrous iron bearing nanoparticles in glacial sediments. *Earth Planet. Sci. Lett*. **493**, 92–101. https://doi.org/10.1016/j.epsl.2018.04.022

Hedges J.I., Keil R.G. (1995) Sedimentary organic matter preservation: an assessment and speculative synthesis. *Mar. Chem*. **49**, 81–115.

Hedges J.I., Keil R.G., Benner R. (1997) What happens to terrestrial organic matter in the ocean? *Org. Geochem*. **27**, 195–212.

Hegseth E.N., Tverberg V. (2013) Effect of Atlantic water inflow on timing of the phytoplankton spring bloom in a high Arctic fjord (Kongsfjorden, Svalbard). *J. Mar. Syst*. **113–114**, 94–105. https://doi.org/10.1016/j.jmarsys.2013.01.003

Helz G.R., Miller C. V., Charnock J.M., Mosselmans J.F.W., Pattrick R.A.D., Garner C.D., Vaughan D.J. (1996) Mechanism of molybdenum removal from the sea and its concentration in black shales: EXAFS evidence. *Geochim. Cosmochim. Acta* **60**, 3631–3642. https://doi.org/10.1016/0016-7037(96)00195-0

Hjelle A. (1993) *The Geology of Svalbard*. Norsk Polarinstitut, Oslo.

Hodal H., Falk-Petersen S., Hop H., Kristiansen S., Reigstad M. (2012) Spring bloom dynamics in Kongsfjorden, Svalbard: Nutrients, phytoplankton, protozoans and primary production. *Polar Biol*. **35**, 191–203. https://doi.org/10.1007/s00300-011-1053-7

Hodson A., Anesio A.M., Tranter M., Fountain A., Osborn M., Priscu J., Laybourn-Parry J., Sattler B. (2008) Glacial Ecosystems. *Ecol. Monogr*. **78**, 41–67. https://doi.org/10.1890/07-0187.1

Hop H., Pearson T., Hegseth E.N., Kovacs K.M., Wiencke C., Kwasniewski S., Eiane K., Mehlum F., Gulliksen B., Wlodarska-Kowalczuk M., Lydersen C., Weslawski J.M., Cochrane S., Gabrielsen G.W., Leakey R.J.G., Lønne O.J., Zajaczkowski M., Falk-Petersen S., Kendall M., Wängberg S.Å., Bischof K., Voronkov A.Y., Kovaltchouk N.A., Wiktor J., Poltermann M., Di Prisco G., Papucci C., Gerland S. (2002) The marine ecosystem of Kongsfjorden, Svalbard. *Polar Res*. **21**, 167–208. https://doi.org/10.1111/j.1751-8369.2002.tb00073.x

Huerta-Diaz M.A., Morse, J.W. (1992) Pyritization of trace metals in anoxic marine sediments. *Geochim. Cosmochim. Acta* **56**, 2681–2702.

Iversen N., Jørgensen B.B. (1993) Diffusion coefficients of sulfate and methane in marine sediments: Influence of porosity. *Geochim. Cosmochim. Acta* **57**, 571–578. https://doi.org/10.1016/0016-7037(93)90368-7

Jones G.A., Kaiteris P. (1983) A vacuum-gasometric technique for rapid and precise analysis of calcium carbonate in sediments and soils. *J. Sediment. Petrol*. **53**, 655–660.

Jørgensen B.B. (1977) The sulfur cycle of a coastal marine sediment (Limfjorden, Denmark). *Limnol. Oceanogr*. **22**, 814–832. https://doi.org/10.4319/lo.1977.22.5.0814

Jørgensen B.B. (1978) A comparison of methods for the quantification of bacterial sulfate reduction in coastal marine sediments. *Geomicrobiol. J*. **1**, 11–27. https://doi.org/10.1080/01490457809377721

Jørgensen B.B. (1982) Mineralization of organic matter in the sea bed—the role of sulphate reduction. *Nature* **296**, 643–645. https://doi.org/10.1038/296643a0

Jørgensen B.B., Nelson D.C. (2004) Sulfide oxidation in marine sediments: Geochemistry meets microbiology, In: *Geochemical Society of America Special Papers* **379**, 63–81.

Kanneworff, E., Nicolaisen, W. (1983) A simple, hand-operated quantitative bottom sampler. *Ophelia* **22**, 253-255.

Kaštovská K., Stibal M., Šabacká M., Černá B., Šantrůčková H., Elster J. (2007) Microbial community structure and ecology of subglacial sediments in two polythermal Svalbard glaciers characterized by epifluorescence microscopy and PLFA. *Polar Biol*. **30**, 277–287. https://doi.org/10.1007/s00300-006-0181-y

Keimowitz A.R., Mailloux B.J., Cole P., Stute M., Simpson H.J., Chillrud S.N. (2007) Laboratory investigations of enhanced sulfate reduction as a groundwater arsenic remediation strategy. *Environ. Sci. Technol*. **41**, 6718–6724. https://doi.org/10.1021/ES061957Q

Kempf P., Forwick M., Laberg J.S., Vorren T.O. (2013) Late Weichselian and Holocene sedimentary palaeoenvironment and glacial activity in the high-arctic van Keulenfjorden, Spitsbergen. *Holocene* **23**, 1607–1618. https://doi.org/10.1177/0959683613499055

Kim J.-H., Peterse F., Willmott V., Kristensen D.K., Baas M., Schouten S., Sinninghe Damsté J.S. (2011) Large ancient organic matter contributions to Arctic marine sediments (Svalbard). *Limnol. Oceanogr*. **56**, 1463–1474. https://doi.org/10.4319/lo.2011.56.4.1463

Kirk M.F., Roden E.E., Crossey L.J., Brealey A.J., Spilde M.N. (2010) Experimental analysis of arsenic precipitation during microbial sulfate and iron reduction in model aquifer sediment reactors. *Geochim. Cosmochim. Acta* **74**, 2538–2555. https://doi.org/10.1016/j.gca.2010.02.002

Klinkhammer G.P., Palmer M.R. (1991) Uranium in the oceans: Where it goes and why. *Geochim. Cosmochim. Acta* **55**, 1799–1806.

Kocar B.D., Borch T., Fendorf S. (2010) Arsenic repartitioning during biogenic sulfidization and transformation of ferrihydrite. *Geochim. Cosmochim. Acta* **74**, 980–994. https://doi.org/10.1016/j.gca.2009.10.023

Kohler J., James T.D., Murray T., Nuth C., Brandt O., Barrand N.E., Aas H.F., Luckman A. (2007) Acceleration in thinning rate on western Svalbard glaciers. *Geophys. Res. Lett*. **34**, LI8502. https://doi.org/10.1029/2007GL030681

Kondo Y., Obata H., Hioki N., Ooki A., Nishino S., Kikuchi, T., Kuma, K. (2016) Transport of trace metals (Mn, Fe, Ni, Zn and Cd) in the western Arctic Ocean (Chukchi Sea and Canada Basin) in late summer 2012. *Deep Sea Res*. **116**, 236–252. https://doi.org/10.1016/j.dsr.2016.08.010

Kostka J.E., Thamdrup B., Glud R.N., Canfield D.E. (1999) Rates and pathways of carbon oxidation in permanently cold Arctic sediments. *Mar. Ecol. Prog. Ser*. **180**, 7–21.

Koziorowska K., Kuliński K., Pempkowiak J. (2016) Sedimentary organic matter in two Spitsbergen fjords: Terrestrial and marine contributions based on carbon and nitrogen contents and stable isotopes composition. *Cont. Shelf Res*. **113**, 38–46. https://doi.org/10.1016/J.CSR.2015.11.010

Ku T.-L., Knauss K.G., Mathieu G.G. (1977) Uranium in open ocean: concentration and isotopic composition. *Deep Sea Res*. **24**, 1005–1017.

Kuliński K., Kędra M., Legeżyńska J., Gluchowska M., Zaborska A. (2014) Particulate organic matter sinks and sources in high Arctic fjord. *J. Mar. Syst*. **139**, 27–37. https://doi.org/10.1016/J.JMARSYS.2014.04.018

Larsen J.N., Anisimov O.A., Constable A., Hollowed A.B., Maynard N., Prestrud P., Prowse T.D., Stone J.M.R. (2014): Polar regions. In: *Climate Change 2014: Impacts, Adaptation, and Vulnerability*. Part B: Regional Aspects. Contribution of Working Group II to the Fifth Assessment Report of the Intergovernmental Panel on Climate Change [Barros, V.R., C.B. Field, D.J. Dokken, M.D. Mastrandrea, K.J. Mach, T.E. Bilir, M. Chatterjee, K.L. Ebi, Y.O. Estrada, R.C. Genova, B. Girma, E.S. Kissel, A.N. Levy, S. MacCracken, P.R. Mastrandrea, and L.L. White (eds.)]. Cambridge University Press, Cambridge, United Kingdom and New York, NY, USA, pp. 1567-1612.

Lalande C., Moriceau B., Leynaert A., Morata N. (2016) Spatial and temporal variability in export fluxes of biogenic matter in Kongsfjorden. *Polar Biol.* **39**, 1725–1738. https://doi.org/10.1007/s00300-016-1903-4

Little S.H., Vance D., Lyons T.W., McManus J. (2015) Controls on trace metal authigenic enrichment in reducing sediments: Insights from modern oxygen-deficient settings. *Am. J. Sci.* **315**, 77–119. https://doi.org/10.2475/02.2015.01

Lovell H., Benn D.I., Lukas S., Ottesen D., Luckman A., Hardiman M., Barr I.D., Boston C.M. and Sevestre H. (2018) Multiple Late Holocene surges of a High-Arctic tidewater glacier system in Svalbard. *Quat. Sci. Rev.* **201**, 162–185.

Lovley D.R. (1993) Dissimilatory Metal Reduction. *Annu. Rev. Microbiol*. **47**, 263–290. https://doi.org/10.1146/annurev.mi.47.100193.001403

Lovley D.R., Phillips E.J.P. (1992) Reduction of Uranium by Desulfovibrio desulfuricans. *Appl. Environ. Microbiol*. **58**, 850–856.

Lovley D.R., Phillips E.J.P., Gorby Y.A., Landa E.R. (1991) Microbial reduction of uranium. *Nature* **350**, 413–416. https://doi.org/10.1038/350413a0

Luther G.W., Howarth R.W., Ryans R.A. (1982) Pyrite and oxidized iron mineral phases formed from pyrite oxidation in salt marsh and estuarine sediments. *Geochim. Cosmochim. Acta* **46**, 2665–2669.

Manceau A., Drits V.A., Silvester E., Bartoli C., Lanson B. (1997) Structural mechanism of Co2+ oxidation by the phyllomanganate buserite. *Am. Mineral*. **82**, 1150–1175. https://doi.org/10.2138/am-1997-11-1213

Manceau A., Gorshkov A.I., Drits V.A. (1992) Structural chemistry of Mn, Fe, Co, and Ni in manganese hydrous oxides: Part II. Information from EXAFS spectroscopy and electron and X-ray diffraction. *Am. Mineral*. **77**, 1144–1157.

März C., Stratmann A., Matthiessen J., Meinhardt A.-K., Eckert S., Schnetger B., Vogt C., Stein R., Brumsack H.-J. (2011) Manganese-rich brown layers in Arctic Ocean sediments:

Composition, formation mechanisms, and diagenetic overprint. *Geochim. Cosmochim. Acta* **75**, 7668–7687. https://doi.org/10.1016/J.GCA.2011.09.046

McKee B.A., DeMaster D.J., Nittrouer C.A. (1987) Uranium geochemistry on the Amazon shelf: Evidence for uranium release from bottom sediments. *Geochim. Cosmochim. Acta* **51**, 2779–2786.

McManus J., Berelson W.M., Klinkhammer G.P., Hammond D.E., Holm C. (2005) Authigenic uranium: Relationship to oxygen penetration depth and organic carbon rain. *Geochim. Cosmochim. Acta* **69**, 95–108. https://doi.org/10.1016/j.gca.2004.06.023

Meinhardt A.K., März C., Schuth S., Lettmann K.A., Schnetger B., Wolff J.O. and Brumsack H.J. (2016) Diagenetic regimes in Arctic Ocean sediments: Implications for sediment geochemistry and core correlation. *Geochim. Cosmochim. Acta* **188**, 125–146.

Meyers P.A. (1990) Impacts of late Quaternary fluctuations in water level on the accumulation of sedimentary organic matter in Walker Lake, Nevada. *Palaeogeogr. Palaeoclimatol. Palaeoecol*. **78**, 229–240. https://doi.org/10.1016/0031-0182(90)90216-T

Middelburg J.J., van der Weijden C.H., Woittiez J.R.W. (1988) Chemical processes affecting the mobility of major, minor and trace elements during weathering of granitic rocks. *Chem. Geol*. **68**, 253–273. https://doi.org/10.1016/0009-2541(88)90025-3

Mitchell P.I., Holm E., Dahlgaard H., Boust D., Leonard K.S., Papucci C., Salbu B., Christensen G., Strand P., Sánchez-Cabeza J.A., Rissanen K., Pollard D., Gascó C. (1999) Radioecological Assessment of the Consequences of Contamination of Arctic Waters : Modelling the Key Processes Controlling Radionuclide Behaviour Under Extreme Conditions (ARMARA).

Mitchell A. C., Brown G.H., Fuge R. (2001) Minor and trace element export from a glacierized Alpine headwater catchment (Haut Glacier d'Arolla, Switzerland). *Hydrol. Process*. **15**, 3499–3524. https://doi.org/10.1002/hyp.1041

Mitchell A.C., Brown G.H., Fuge R. (2006) Minor and trace elements as indicators of solute provenance and flow routing in a subglacial hydrological system. *Hydrol. Process*. **20**, 877–897. https://doi.org/10.1002/hyp.6112

Monien P., Lettmann K.A., Monien D., Asendorf S., Wölfl A.-C., Lim C.H., Thal J., Schnetger B., Brumsack H.J. (2014) Redox conditions and trace metal cycling in coastal sediments from the maritime Antarctic. *Geochim. Cosmochim. Acta* **141**, 26–44. https://doi.org/10.1016/j.gca.2014.06.003

Montross S.N., Skidmore M., Tranter M., Kivimäki A.-L., Parkes R.J. (2012) A microbial driver of chemical weathering in glaciated systems. *Geology* **41**, 215–218. https://doi.org/10.1130/G33572.1

Morel F.M.M., Hudson R.J.M., Price N.M. (1991) Limitation of productivity by trace metals in the sea. *Limnol. Ocean*. **36**, 1742–1755.

Morel F.M.M., Price N.M. (2003) The biogeochemical cycles of trace metals in the oceans. *Science* **300**, 944–947. https://doi.org/10.1126/science.1083545

Morford J.L., Emerson S. (1999) The geochemistry of redox sensitive trace metals in sediments. *Geochim. Cosmochim. Acta* **63**, 1735–1750. https://doi.org/10.1016/S0016-7037(99)00126-X

Morford J.L., Martin W.R., Carney C.M. (2009) Uranium diagenesis in sediments underlying bottom waters with high oxygen content. *Geochim. Cosmochim. Acta* **73**, 2920–2937. https://doi.org/10.1016/j.gca.2009.02.014

Morse J.W., Luther III G.W. (1999) Chemical influences on trace metal-sulfide interactions in

anoxic sediments. *Geochim. Cosmochim. Acta* **63**, 3373–3378.
Müller P.J. (1977) C/N ratios in Pacific deep-sea sediments: Effect of inorganic ammonium and organic nitrogen compounds sorbed by clays. *Geochim. Cosmochim. Acta* **41**, 765–776.
Murray J.W., Dillard J.G. (1979) The oxidation of cobalt(II) adsorbed on manganese dioxide. *Geochim. Cosmochim. Acta* **43**, 781–787. https://doi.org/10.1016/0016-7037(79)90261-8
Murray K.J., Webb S.M., Bargar J.R., Tebo B.M. (2007) Indirect oxidation of Co(II) in the presence of the marine Mn(II)-oxidizing bacterium Bacillus sp. strain SG-1. *Appl. Environ. Microbiol*. **73**, 6905–6909. https://doi.org/10.1128/AEM.00971-07
Nameroff T.J., Calvert S.E., Murray J.W. (2004) Glacial-interglacial variability in the eastern tropical North Pacific oxygen minimum zone recorded by redox-sensitive trace metals. *Paleoceanography* **19**, PA1010. https://doi.org/10.1029/2003PA000912
Nickel M., Vandieken V., Brüchert V., Jørgensen B.B. (2008) Microbial Mn(IV) and Fe(III) reduction in northern Barents Sea sediments under different conditions of ice cover and organic carbon deposition. *Deep. Res. II* **55**, 2390–2398. https://doi.org/10.1016/j.dsr2.2008.05.003
Nielsdóttir M.C., Moore C.M., Sanders R., Hinz D.J., Achterberg E.P. (2009) Iron limitation of the postbloom phytoplankton communities in the Iceland Basin. *Glob. Biogeochem. Cycles* **23**, GB3001. https://doi.org/10.1029/2008GB003410
Nixon S.L., Telling J.P., Wadham J.L., Cockell C.S. (2017) Viable cold-tolerant iron-reducing microorganisms in geographically diverse subglacial environments. *Biogeosciences* **14**, 1445–1455. https://doi.org/10.5194/bg-14-1445-2017
Onarheim I.H., Smedsrud L.H., Ingvaldsen R.B., Nilsen F. (2014) Loss of sea ice during winter north of Svalbard. *Tellus, Ser. A Dyn. Meteorol. Oceanogr*. **66**, 23933. https://doi.org/10.3402/tellusa.v66.23933
Öztürk M. (1995) Trends of trace metal (Mn, Fe, Co, Ni, Cu, Zn, Cd, and Pb) distributions at the oxic-anoxic interface in sulfides water of the Drammensjord. *Mar. Chem*. **48**, 329–342.
Pattrick R.A.D., Mosselmans J.F.W., Charnock J.M., England K.E.R., Helz G.R., Garner C.D., Vaughan D.J. (1997) The structure of amorphous copper sulfide precipitates: An X-ray absorption study, *Geochim. Cosmochim. Acta* **61**, 2023-2036.
Peacock C.L., Sherman D.M. (2004) Copper(II) sorption onto goethite, hematite and lepidocrocite: A surface complexation model based on ab initio molecular geometries and EXAFS spectroscopy. *Geochim. Cosmochim. Acta* **68**, 2623–2637. https://doi.org/10.1016/j.gca.2003.11.030
Peacock C. L. and Sherman D. M. (2007) Sorption of Ni by birnessite: Equilibrium controls on Ni in seawater. *Chem. Geol.* **238**, 94–106.
Postma D. (1985) Concentration of Mn and separation from Fe in sediments—I. Kinetics and stoichiometry of the reaction between birnessite and dissolved Fe(II) at 10°C. *Geochim. Cosmochim. Acta* **49**, 1023–1033. https://doi.org/10.1016/0016-7037(85)90316-3
Postma D., Appelo C.A.J. (2000) Reduction of Mn-oxides by ferrous iron in a flow system: Column experiment and reactive transport modeling. *Geochim. Cosmochim. Acta* **64**, 1237–1247.
Poulson R.L., Siebert C., McManus J., Berelson W.M. (2006) Authigenic molybdenum isotopes signatures in marine sediments. *Geology* **34**, 617–620.
Poulton S.W., Canfield D.E. (2005) Development of a sequential extraction procedure for iron: Implications for iron partitioning in continentally derived particulates. *Chem. Geol*. **214**, 209–221. https://doi.org/10.1016/j.chemgeo.2004.09.003

Prahl F.G., Bennett J.T., Carpenter R. (1980) The early diagenesis of aliphatic hydrocarbons and organic matter in sedimentary particulates from Dabob Bay, Washington. *Geochim. Cosmochim. Acta* **44**, 1967–1976. https://doi.org/10.1016/0016-7037(80)90196-9

Prahl F.G., De Lange G.J., Scholten S., Cowie G.L. (1997) A case of post-depositional aerobic degradation of terrestrial organic matter in turbidite deposits from the Madeira Abyssal Plain. *Org. Geochem*. **27**, 141–152.

Raiswell R., Tranter M., Benning L.G., Siegert M., De'ath R., Huybrechts P., Payne T. (2006) Contributions from glacially derived sediment to the global iron (oxyhydr)oxide cycle: Implications for iron delivery to the oceans. *Geochim. Cosmochim. Acta* **70**, 2765–2780. https://doi.org/10.1016/J.GCA.2005.12.027

Redfield A. C. (1934) On the proportions of organic derivatives in seawater and their relation to the composition of plankton. *James Johnstone Memorial Volume*, 176-192.

Richard D., Sundby B., Mucci A. (2013) Kinetics of manganese adsorption, desorption, and oxidation in coastal marine sediments. *Limnol. Oceanogr*. **58**, 987–996. https://doi.org/10.4319/lo.2013.58.3.0987

Riedinger N., Formolo M.J., Lyons T.W., Henkel S., Beck A., Kasten S. (2014) An inorganic geochemical argument for coupled anaerobic oxidation of methane and iron reduction in marine sediments. *Geobiology* **12**, 172–181. https://doi.org/10.1111/gbi.12077

Ritchie J.C., Mchenry J.R. (1990) Application of radioactive fallout cesium-137 for measuring soil erosion and sediment accumulation rates and patterns: A review. *J. Environ. Qual*. **19**, 215–233.

Rijkenberg M.J.A., Slagter H.A., van der Loeff M.R., van Ooije J., Gerringa, L.J.A. (2018) Dissolved Fe in the deep and upper Arctic Ocean with a focus on Fe limitation in the Nansen Basin. *Front. Mar. Sci*. **5**, 88. https://doi.org/10.3389/fmars.2018.00088

Robador A., Brüchert V., Jørgensen B.B. (2009) The impact of temperature change on the activity and community composition of sulfate-reducing bacteria in arctic versus temperate marine sediments. *Environ. Microbiol*. **11**, 1692–1703. https://doi.org/10.1111/j.1462-2920.2009.01896.x

Robbins L.J., Lalonde S.V., Planavsky N.J., Partin C.A., Reinhard C.T., Kendall B., Scott, C., Hardist D.S., Gill B.C., Alessi D.S., Dupont C.L., Saito M.A., Crowe S.A., Poulton S.W., Bekker A., Lyons T.W., Konhauser K.O. (2016) Trace elements at the intersection of marine biological and geochemical evolution. *Earth-Science Rev*. **163**, 323–348. https://doi.org/10.1016/J.EARSCIREV.2016.10.013

Rowan D.E., Péwé T.L., Péwé R.H., Stuckenrath R. (1982) Holocene glacial geology of the Svea Lowland, Spitsbergen, Svalbard. *Geogr. Ann. Ser. A, Phys. Geogr*. **64**, 35–51.

Røy H., Weber H.S., Tarpgaard I.H., Ferdelman T.G., Jørgensen B.B. (2014) Determination of dissimilatory sulfate reduction rates in marine sediment via radioactive 35 S tracer. *Limnol. Oceanogr*. *Methods* **12**, 196–211. https://doi.org/10.4319/lom.2014.12.196

Sagemann J., Jørgensen B.B., Greeff O. (1998.) Temperature dependence and rates of sulfate reduction in cold sediments of Svalbard, Arctic Ocean. *Geomicrobiol. J*. 15, 85–100.

Schippers A., Jørgensen B.B. (2002) Biogeochemistry of pyrite and iron sulfide oxidation in marine sediments. *Geochim. Cosmochim. Acta* **66**, 85–92. https://doi.org/10.1016/S0016-7037(01)00745-1

Schmidt F., Hinrichs K.-U., Elvert M. (2010) Sources, transport, and partitioning of organic matter at a highly dynamic continental margin. *Mar. Chem*. **118**, 37–55. https://doi.org/10.1016/J.MARCHEM.2009.10.003

Scholz F., Severmann S., McManus J., Hensen C. (2014a) Beyond the Black Sea paradigm: The sedimentary fingerprint of an open-marine iron shuttle. *Geochim. Cosmochim. Acta* **127**, 368–380. https://doi.org/10.1016/j.gca.2013.11.041

Scholz F., Severmann S., McManus J., Noffke A., Lomnitz U., Hensen C. (2014b) On the isotope composition of reactive iron in marine sediments: Redox shuttle versus early diagenesis. *Chem. Geol*. **389**, 48–59. https://doi.org/10.1016/J.CHEMGEO.2014.09.009

Schulz H.D., Zabel M. (Eds.) (2006) *Marine Geochemistry*. Springer-Verlag, Heidelberg.

Seeberg-Elverfeldt J., Schlüter M., Feseker T., Kölling M. (2005) Rhizon sampling of porewaters near the sediment-water interface. *Limnol. Oceanogr. Methods* **3**, 361–371.

Sharp M., Parkes J., Fairchild I.J., Lamb H., Tranter M. (1999) Widespread bacterial populations at glaciers beds and their relationship to rock weathering and carbon cycling. *Geology* **27**, 107–110. https://doi.org/10.1130/0091-7613(1999)027<0107:WBPAGB>2.3.CO

Sharp M., Tranter M., Brown G.H., Skidmore M, (1995) Rates of chemical denudation and CO2 drawdown in a glacier-covered alpine catchment. *Geology* **23**, 61–64.

Shaw T.J., Gieskes J.M., Jahnke R.A. (1990) Early diagenesis in differing depositional environments: The response of transition metals in pore water. *Geochim. Cosmochim. Acta* **54**, 1233–1246. https://doi.org/10.1016/0016-7037(90)90149-F

Sherman D.M., Peacock C.L. (2010) Surface complexation of Cu on birnessite (d-MnO2): Controls on Cu in the deep ocean. *Geochim. Cosmochim. Acta* **74**, 6721–6730. https://doi.org/10.1016/j.gca.2010.08.042

Shimmield G., Price N. (1986) The behaviour of molybdenum and manganese during early sediment diagenesis — offshore Baja California, Mexico. *Mar. Chem*. **19**, 261–280. https://doi.org/10.1016/0304-4203(86)90027-7

Skrabal S.A., Donat J.R., Burdige D.J. (2000) Pore water distributions of dissolved copper and copper-complexing ligands in estuarine and coastal marine sediments. *Geochim. Cosmochim. Acta* **64**, 1843–1857.

Solheim A., Pfirman S.L. (1985) Sea-floor morphology outside a grounded, surging glacier; Bråsvellbreen, Svalbard. *Mar. Geol*. **65**, 127–143. https://doi.org/10.1016/0025-3227(85)90050-7

Spielhagen R.F., Werner K., Sørensen S.A., Zamelczyk K., Kandiano E., Budeus G., Husum K., Marchitto T.M., Hald M., Wegener A. (2011) Enhanced Modern Heat Transfer to the Arctic by Warm Atlantic Water. *Science* **331**, 450–453. https://doi.org/10.1126/science.1199421

Statham P.J., Skidmore M., Tranter M. (2008) Inputs of glacially derived dissolved and colloidal iron to the coastal ocean and implications for primary productivity. *Global Biogeochem. Cycles* **22**, GB3013. https://doi.org/10.1029/2007GB003106

Stockdal A., Davison W., Zhang H., Hamilton-Taylor J. (2010) The association of cobalt with iron and manganese (oxyhydr)oxides in marine sediment. *Aquat. Geochemistry* **16**, 575–585. https://doi.org/10.1007/s10498-010-9092-1

Suess E. (1979) Mineral phases formed in anoxic sediments by microbial decomposition of organic matter. *Geochim. Cosmochim. Acta* **43**, 339–352. https://doi.org/10.1016/0016-7037(79)90199-6

Sun Y.-Z., Püttmann W. (2000) The role of organic matter during copper enrichment in Kupferschiefer from the Sangerhausen basin, Germany. *Org. Geochem*. **31**, 1143–1161.

Sund M., Eiken T. (2010) Recent surges on Blomstrandbreen, Comfortlessbreen and Nathorstbreen, Svalbard. *J. Glaciol*. **56**, 182–184.

Sunda W.G. (2012) Feedback interactions between trace metal nutrients and phytoplankton in

the ocean. *Front. Microbiol*. **3**, 204. https://doi.org/10.3389/fmicb.2012.00204

Svendsen H., Beszczynska-Møller A., Hagen J.O., Lefauconnier B., Tverberg V.G.S., Ørbæck J.B., Bischof K., Papucci C., Zajaczkowski M., Azzolini R., Bruland O., Wienck, C., Winther J.G., Dallmann W. (2002) The physical environment of Kongsfjorden-Krossfjorden, an Arctic fjord system in Svalbard. *Polar Res*. **21**, 133–166.

Swanner E.D., Planavsky N.J., Lalonde S. V., Robbins L.J., Bekker A., Rouxel O.J., Saito M.A., Kappler A., Mojzsis S.J., Konhauser K.O. (2014) Cobalt and marine redox evolution. *Earth Planet. Sci. Lett*. **390**, 253–263. https://doi.org/10.1016/J.EPSL.2014.01.001

Szczuciński W., Zajączkowski M., Scholten J. (2009) Sediment accumulation rates in subpolar fjords – Impact of post-Little Ice Age glaciers retreat, Billefjorden, Svalbard. *Estuar. Coast. Shelf Sci.* **85**, 345–356. https://doi.org/10.1016/J.ECSS.2009.08.021

Takahashi Y., Manceau A., Geoffroy N., Marcus M.A., Usui A. (2007) Chemical and structural control of the partitioning of Co, Ce, and Pb in marine ferromanganese oxides. *Geochim. Cosmochim. Acta* **71**, 984–1008. https://doi.org/10.1016/j.gca.2006.11.016

Tapia J., Audry S. (2013) Control of early diagenesis processes on trace metal (Cu, Zn, Cd, Pb and U) and metalloid (As, Sb) behaviors in mining- and smelting-impacted lacustrine environments of the Bolivian Altiplano. *Appl. Geochemistry* **31**, 60–78. https://doi.org/10.1016/j.apgeochem.2012.12.006

Tessier A., Campbell P.G.C., Bisson M. (1979) Sequential extraction procedure for the speciation of particulate trace metals. *Anal. Chem*. **51**, 844–851. https://doi.org/10.1021/ac50043a017

Thamdrup B., Fossing H., Jørgensen B.B. (1994) Manganese, iron, and sulfur cycling in a coastal marine sediment. Aarhus Bay, Denmark. *Geochim. Cosmochim. Acta* **58**, 5115–29.

Torres E., Auleda M. (2013) A sequential extraction procedure for sediments affected by acid mine drainage. *J. Geochemical Explor.* **128**, 35–41.

Tovar-Sánchez A., Duarte C.M., Alonso J.C., Lacorte S., Tauler R., Galban-Malagón C. (2010) Impacts of metals and nutrients released from melting multiyear Arctic sea ice. *J. Geophys. Res*. **115**, C07033. https://doi.org/10.1029/2009JC005685

Tranter M. (2003) Geochemical Weathering in Glacial and Proglacial Environments. *Treatise on Geochemistry* **5**, 189-205.

Tranter M., Huybrechts P., Munhoven G., Sharp M.J., Brown G.H., Jones I.W., Hodson A.J., Hodgkins R., Wadham J.L. (2002) Direct effect of ice sheets on terrestrial bicarbonate, sulphate and base cation fluxes during the last glacial cycle: minimal impact on atmospheric CO 2 concentrations. *Chem. Geol*. **190**, 33–44.

Tribovillard N., Algeo T.J., Lyons T., Riboulleau A. (2006) Trace metals as paleoredox and paleoproductivity proxies: An update. *Chem. Geol*. **232**, 12–32. https://doi.org/10.1016/j.chemgeo.2006.02.012

Tucker M.D., Barton L.L., Thomson B.M. (1997) Reduction and immobilization of molybdenum by Desulfovibrio desulfuricans. *J. Environ. Qual*. **26**, 1146–1152. https://doi.org/10.2134/jeq1997.00472425002600040029x

Vandieken V., Nickel M., Jørgensen B.B. (2006) Carbon mineralization in Arctic sediments northeast of Svalbard: Mn(IV) and Fe(III) reduction as principal anaerobic respiratory pathways. *Mar. Ecol. Prog. Ser*. **322**, 15–27. https://doi.org/10.3354/meps322015

Wadham J.L., Bottrell S., Tranter M., Raiswell R. (2004) Stable isotope evidence for microbial sulphate reduction at the bed of a polythermal high Arctic glacier. *Earth Planet. Sci. Lett*. **219**, 341–355. https://doi.org/10.1016/S0012-821X(03)00683-6

Wadham J.L., Cooper R.J., Tranter M., Hodgkins R. (2001) Enhancement of glacial solute fluxes in the proglacial zone of a polythermal glacier. *J. Glaciol*. **47**, 378–386. https://doi.org/10.3189/172756501781832188

Wadham J.L., Tranter M., Skidmore M., Hodson A.J., Priscu J., Lyons W.B., Sharp M., Wynn P., Jackson M. (2010) Biogeochemical weathering under ice: Size matters. *Global Biogeochem. Cycles* **24**, GB3025. https://doi.org/10.1029/2009GB003688

Wehrmann L.M., Formolo M.J., Owens J.D., Raiswell R., Ferdelman T.G., Riedinger N., Lyons T.W. (2014) Iron and manganese speciation and cycling in glacially influenced high-latitude fjord sediments (West Spitsbergen, Svalbard): Evidence for a benthic recycling-transport mechanism. *Geochim. Cosmochim. Acta* **141**, 628–655. https://doi.org/10.1016/j.gca.2014.06.007

Wehrmann L.M., Riedinger N., Brunner B., Kamyshny A., Hubert C.R.J., Herbert L.C., Brüchert V., Jørgensen B.B., Ferdelman T.G., Formolo M.J. (2017) Iron-controlled oxidative sulfur cycling recorded in the distribution and isotopic composition of sulfur species in glacially influenced fjord sediments of west Svalbard. *Chem. Geol*. **466**, 678–695. https://doi.org/10.1016/j.chemgeo.2017.06.013

Widerlund A. (1996) Early diagenetic remobilization of copper in near-shore marine sediments: a quantitative pore-water model. *Mar. Chem*. **54**, 41–53.

Wynn P.M., Hodson A., Heaton T. (2006) Chemical and isotopic switching within the subglacial environment of a High Arctic glacier. *Biogeochemistry* **78**, 173–193. https://doi.org/10.1007/s10533-005-3832-0

Zaborska A., Pempkowiak J., Papucci C. (2006) Some sediment characteristics and sedimentation rates in an Arctic fjord (Kongsfjorden, Svalbard). *Annu. Environ. Prot*. **8**, 79–96.

Zaggia L., Zonta R. (1997) Metal-sulphide formation in the contaminated anoxic sludge of the Venice canals. *Appl. Geochemistry* **12**, 527–536.

Zajączkowski M., Szczuciński W., Bojanowski R. (2004) Recent changes in sediment accumulation rates in Adventfjorden, Svalbard. *Oceanologia* **46**, 217–231.

Zegeye A., Bonneville S., Benning L.G., Sturm A., Fowle D.A., Jones C., Canfield D.E., Ruby C., MacLean L.C., Nomosatryo S., Crowe S.A., Poulton S.W. (2012) Green rust formation controls nutrient availability in a ferruginous water column. *Geology* **40**, 599–602. https://doi.org/10.1130/G32959.1

Zemp M., Huss M., Thibert E., Eckert N., McNabb R., Huber J., Barandun M., Machguth H., Nussbaumer S. U., Gärtner-Roer I., Thomson L., Paul F., Maussion F., Kutuzov S. and Cogley J. G. (2019) Global glacier mass changes and their contributions to sea-level rise from 1961 to 2016. *Nature* **568**, 382–386.

Zheng Y., Anderson R.F., van Geen A., Fleisher M.Q. (2002) Remobilization of authigenic uranium in marine sediments by bioturbation. *Geochim. Cosmochim. Acta* **66**, 1759–1772. https://doi.org/10.1016/S0016-7037(01)00886-9

Zheng Y., Anderson R.F., van Geen A., Kuwabara J. (2000) Authigenic molybdenum formation in marine sediments: a link to pore water sulfide in the Santa Barbara Basin. *Geochim. Cosmochim. Acta* **64**, 4165–4178. https://doi.org/10.1016/S0016-7037(00)00495-6

Ziaja W. (2001) Glacial Recession in Sørkappland and Central Nordenskiöldland, Spitsbergen, Svalbard, during the 20th Century. *Arctic, Antarct. Alp. Res*. **33**, 36–41.

*Figure captions*

**Figure 1.** Map of Van Mijenfjorden (VM) and Van Keulenfjorden (VK) showing the locations of the coring stations (VM-In, -Mid, and -Out, VK- In, -Mid, and -Out) and major meltwater inputs, as listed in Table 1: A) Berseliusdalen, B) Reindalen, C) Kjellströmdalen, D) Paulabreen, E) Danzigdalen, F) Steenstrupdalen, G) Doktorbreen, H) Liestølbreen, I) Nathorstbreen, and J) Penckbreen. References: Hjelle, 1993; Wehrmann et al., 2014; http://svalbardkartet.npolar.no.

**Figure 2.** Profiles of cesium-137 at VM-In (a) and VK-In (d), excess lead-210 at VM-In (b) and VK-In (e), and the natural log of the excess lead-210 at VM-In (c) with a fitted linear regression, from which the sediment accumulation rate was calculated.

**Figure 3.** Sulfate reduction rates with depth at the inner, middle, and outer sites in VM and VK.

**Figure 4.** Depth profiles at the inner, middle, and outer sites of porewater sulfate concentrations in VM (a) and VK (d), acid-volatile sulfide (AVS) content in VM (b) and VK (e), and chromium-reducible sulfur (CRS) content in VM (c) and VK (f).

**Figure 5.** Depth profiles of pore water Fe (open circles) and solid phase Fe content in the acid-soluble, easily reducible, reducible, and oxidizable fractions (connected lines) at VM-In, -Mid, and -Out (a-c) and VK-In, -Mid, and -Out (d-f). The total solid content is the sum of the four fractions and shown as shaded areas.

**Figure 6.** Depth profiles of pore water Mn (open circles) and solid phase Mn content in the exchangeable, acid-soluble, easily reducible, reducible, and oxidizable fractions (connected lines) at VM-In, -Mid, and -Out (a-c) and VK-In, -Mid, and -Out (d-f). The total solid content is the sum of the five fractions and shown as a shaded area.

**Figure 7.** Depth profiles of pore water Co (open circles) and solid phase Co content in the exchangeable, acid-soluble, easily reducible, reducible, and oxidizable fractions (connected lines) at VM-In, -Mid, and -Out (a-c) and VK-In, -Mid, and -Out (d-f). The total solid content is the sum of the five fractions and shown as a shaded area.

**Figure 8.** Depth profiles of pore water Ni (open circles) and solid phase Ni content in the exchangeable, acid-soluble, easily reducible, reducible, and oxidizable fractions (connected lines) at VM-In, -Mid, and -Out (a-c) and VK-In, -Mid, and -Out (d-f). The total solid content is the sum of the five fractions and shown as a shaded area.

**Figure 9.** Depth profiles of pore water Cu (open circles) and solid phase Cu content in the exchangeable, acid-soluble, easily reducible, reducible, and oxidizable fractions (connected lines) at VM-In, -Mid, and -Out (a-c) and VK-In, -Mid, and -Out (d-f). The total solid content is the sum of the five fractions and shown as a shaded area.

**Figure 10.** Depth profiles of pore water U (open circles) and total solid phase U content in the exchangeable, acid-soluble, easily reducible, reducible, and oxidizable fractions (connected lines) at VM-In, -Mid, and -Out (a-c) and VK-In, -Mid, and -Out (d-f). The total solid content is

the sum of the five fractions and shown as a shaded area. Black triangles on the pore water concentration axes indicate average seawater values.

**Figure 11.** Depth profiles of pore water Mo (open circles) and solid phase Mo content in the exchangeable, acid-soluble, easily reducible, reducible, and oxidizable fractions (connected lines) at VM-In, -Mid, and -Out (a-c) and VK-In, -Mid, and -Out (d-f). The total solid content is the sum of the five fractions and shown as a shaded area. Black triangles on the pore water concentration axes indicate average seawater values.

**Figure 12.** Depth profiles of pore water As (open circles) and solid phase As content in the acid-soluble, easily reducible, reducible, and oxidizable fractions (connected lines) at VM-In, -Mid, and -Out (a-c) and VK-In, -Mid, and -Out (d-f). The total solid content is the sum of the four fractions and shown as a shaded area.\

**Figure 13.** A schematic diagram illustrating **a)** differences in source sediment between the two fjords in this study related to glacial input via meltwater streams in VM and a tidewater glacier in VK, **b)** the head-to-mouth gradients in fjord sediment Fe, Mn, and sulfur cycling as controlled by organic carbon availability (i.e. the concentration of labile organic carbon per unit volume of sediment) and sediment accumulation rate, and **c)** the predominant biogeochemical behaviors of Co, Ni, Cu, U, Mo, and As interacting with the Fe/Mn-(oxy)hydroxide (-OHO), sulfide mineral (e.g. monosulfides, pyrite), and pore water pools within the sediment at the glacially influenced inner fjord regions compared to the marine-influenced outer fjord regions.

**Supplemental Figure S1.** Depth profiles of total organic carbon (TOC) and total inorganic carbon (TIC) in dry weight percent at the inner, middle, and outer sites in VM and VK.

**Supplemental Figure S2.** Depth profile of pore water chloride concentrations at the inner, middle, and outer sites in VM and VK.

Journal Pre-proofs

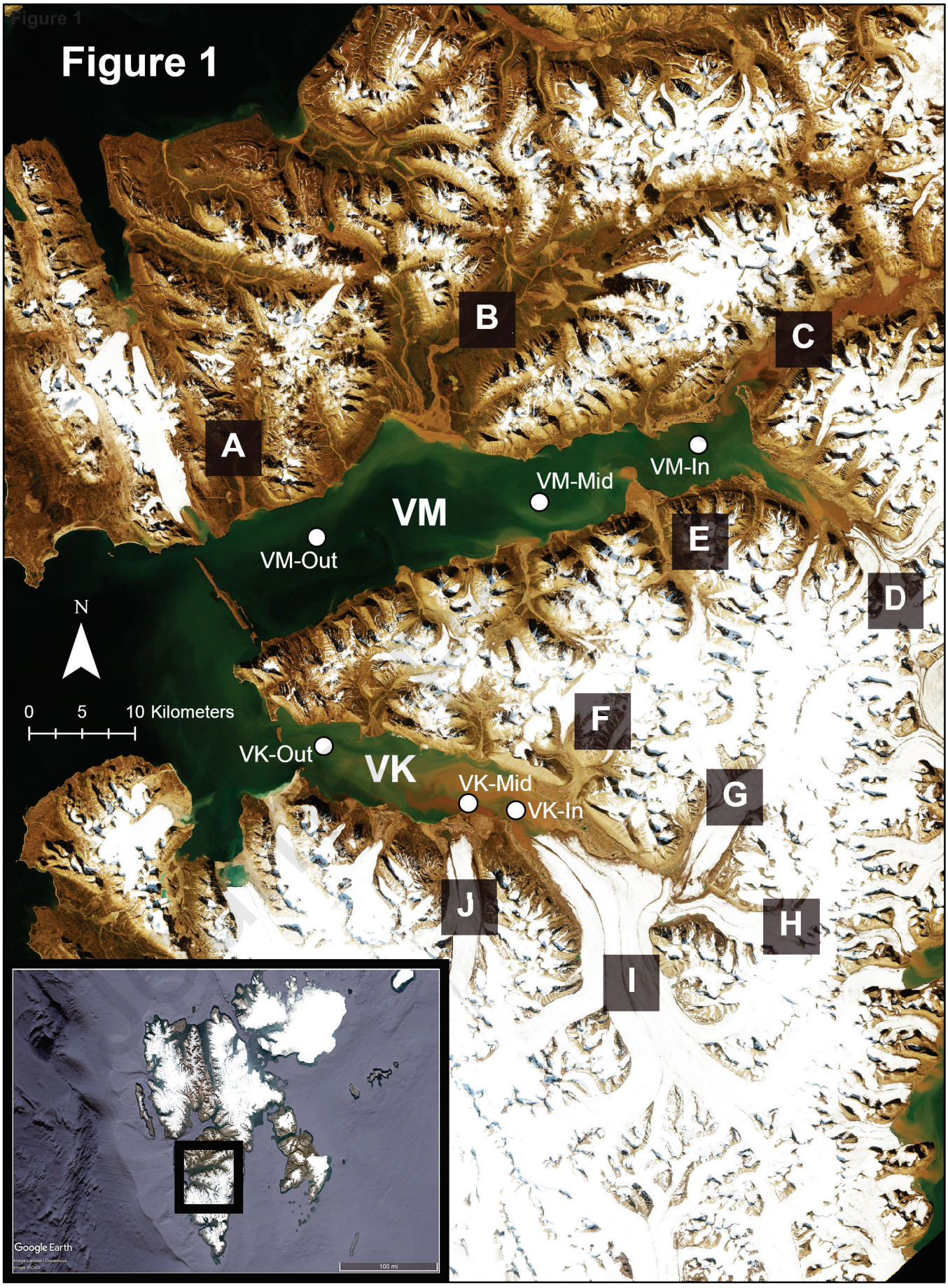
Figure 1
A
B
C
D
E
F
G
H
I
J
VM
VM-In
VM-Mid
VM-Out
VK
VK-Out
VK-Mid
VK-In
N
0 5 10 Kilometers
Google Earth
100 mi

Figure 2

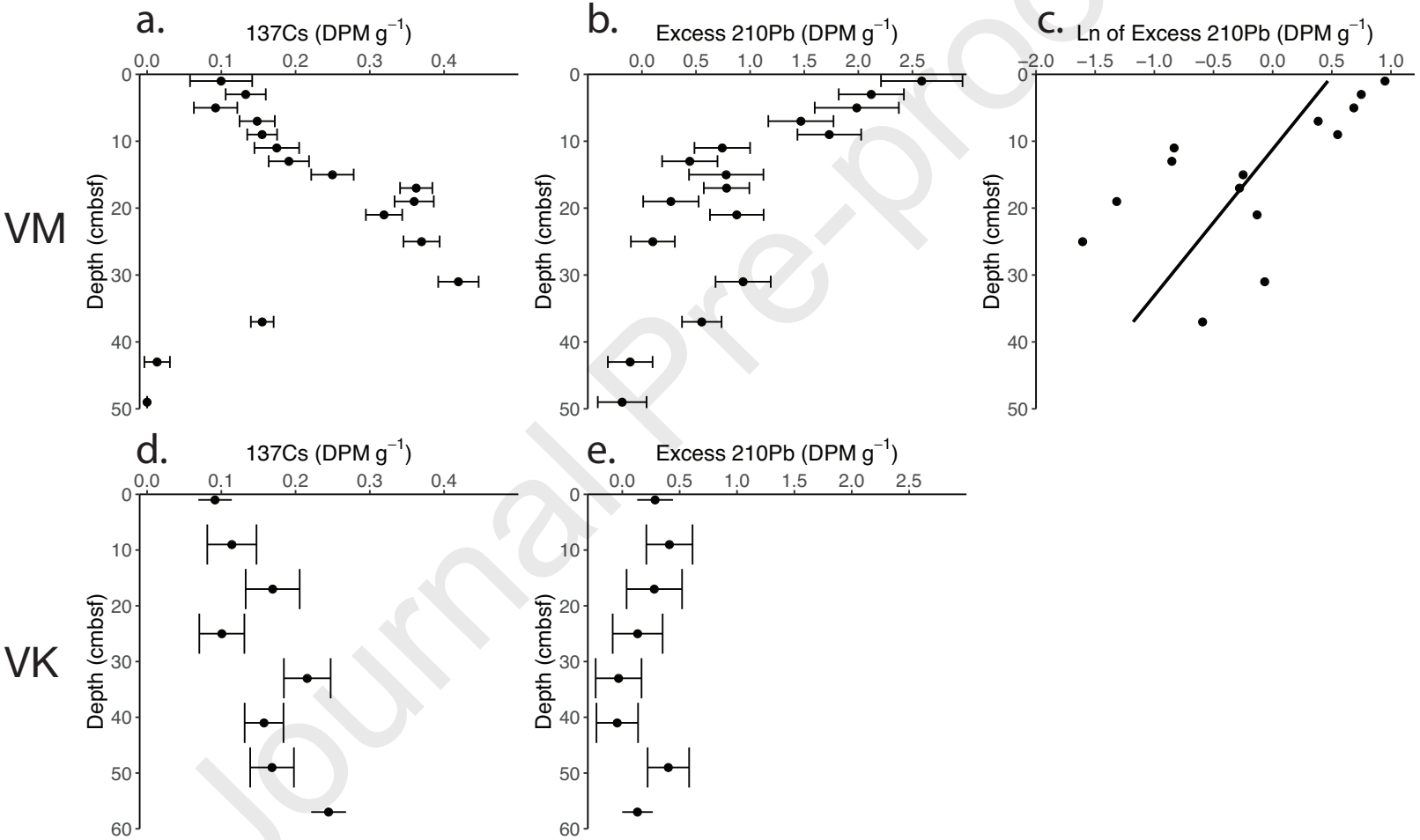


Journal Pre-proofs

Figure 3

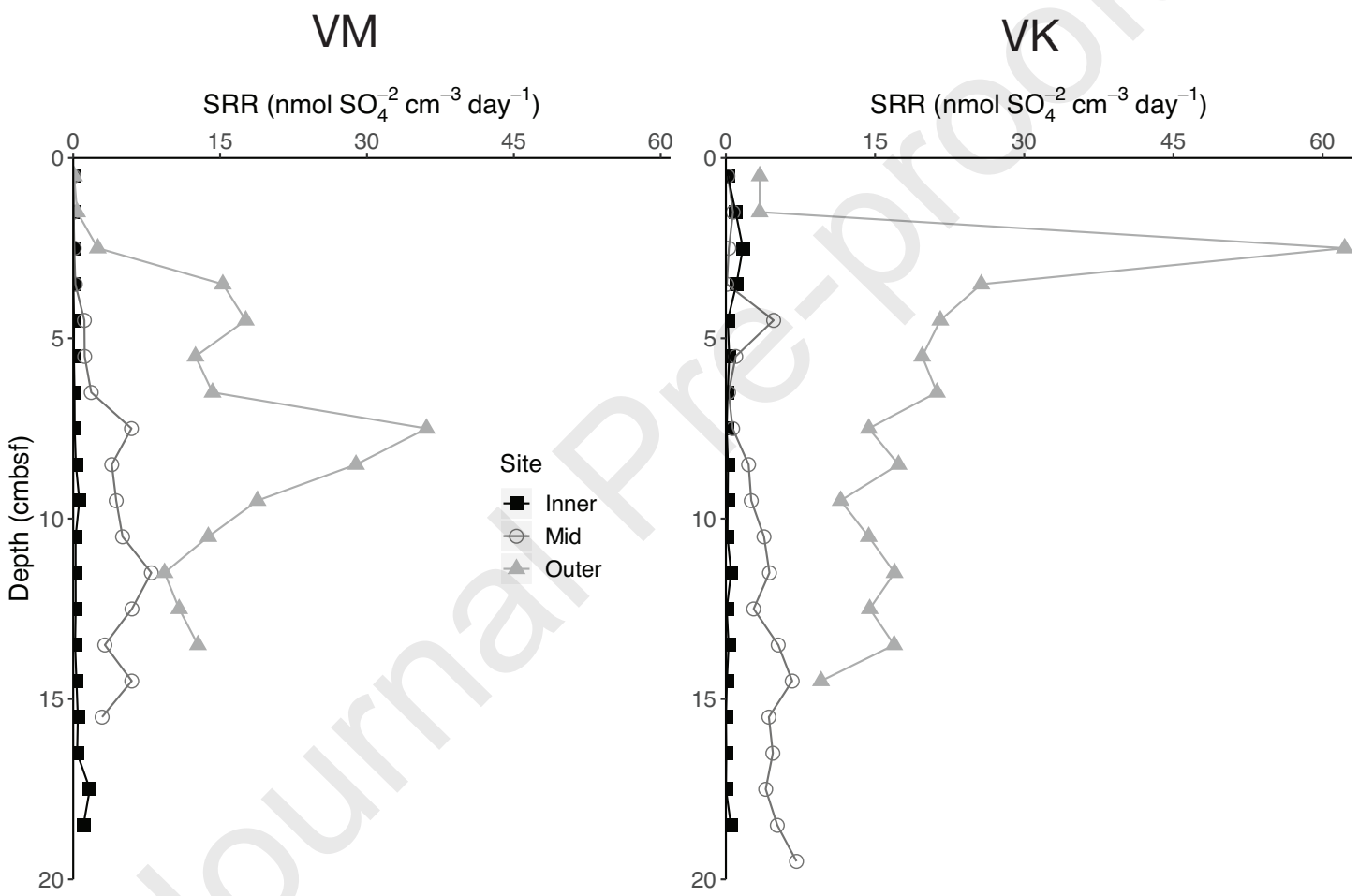


Journal Pre-proofs

Figure 4

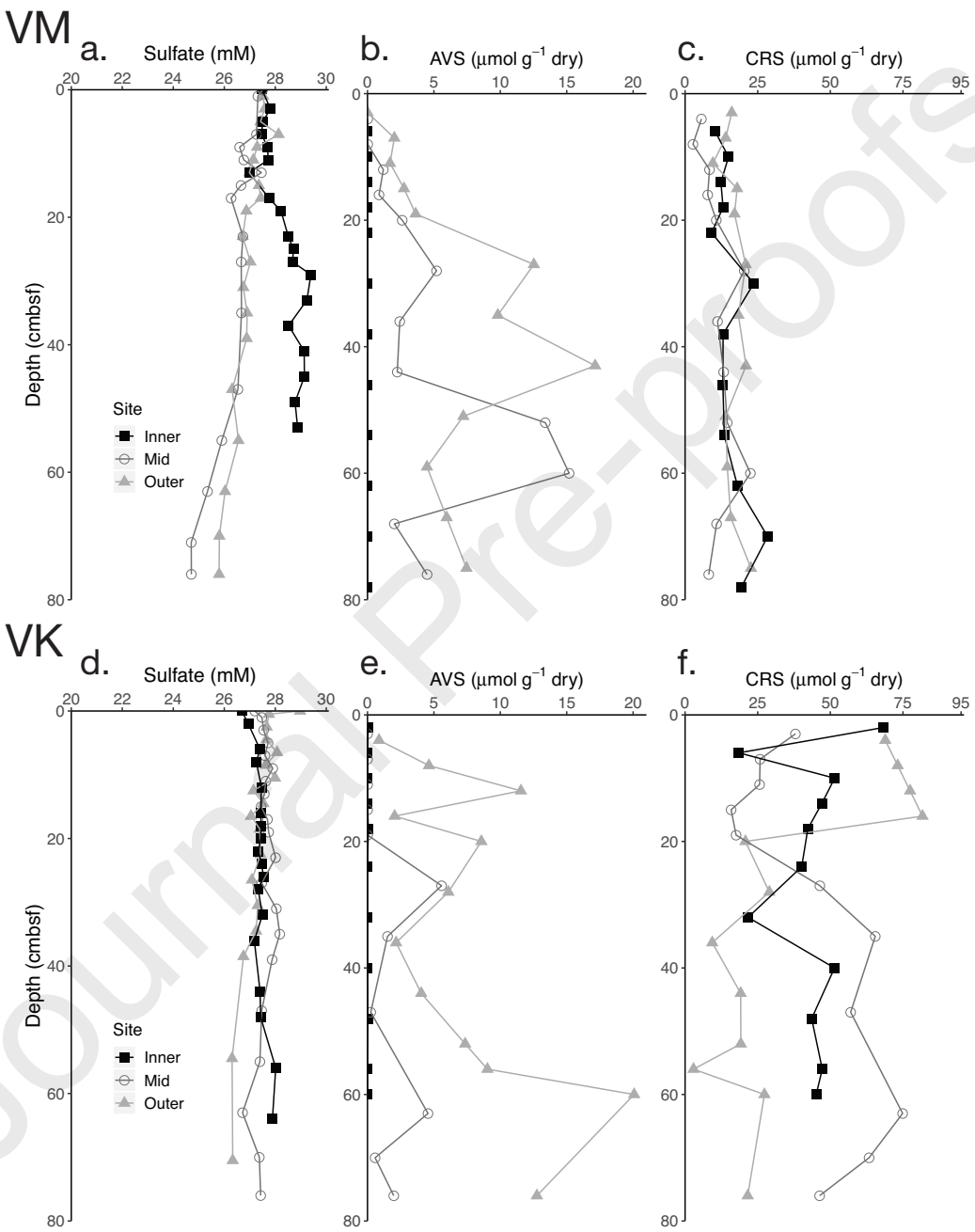


Journal Pre-proofs

# Figure 5

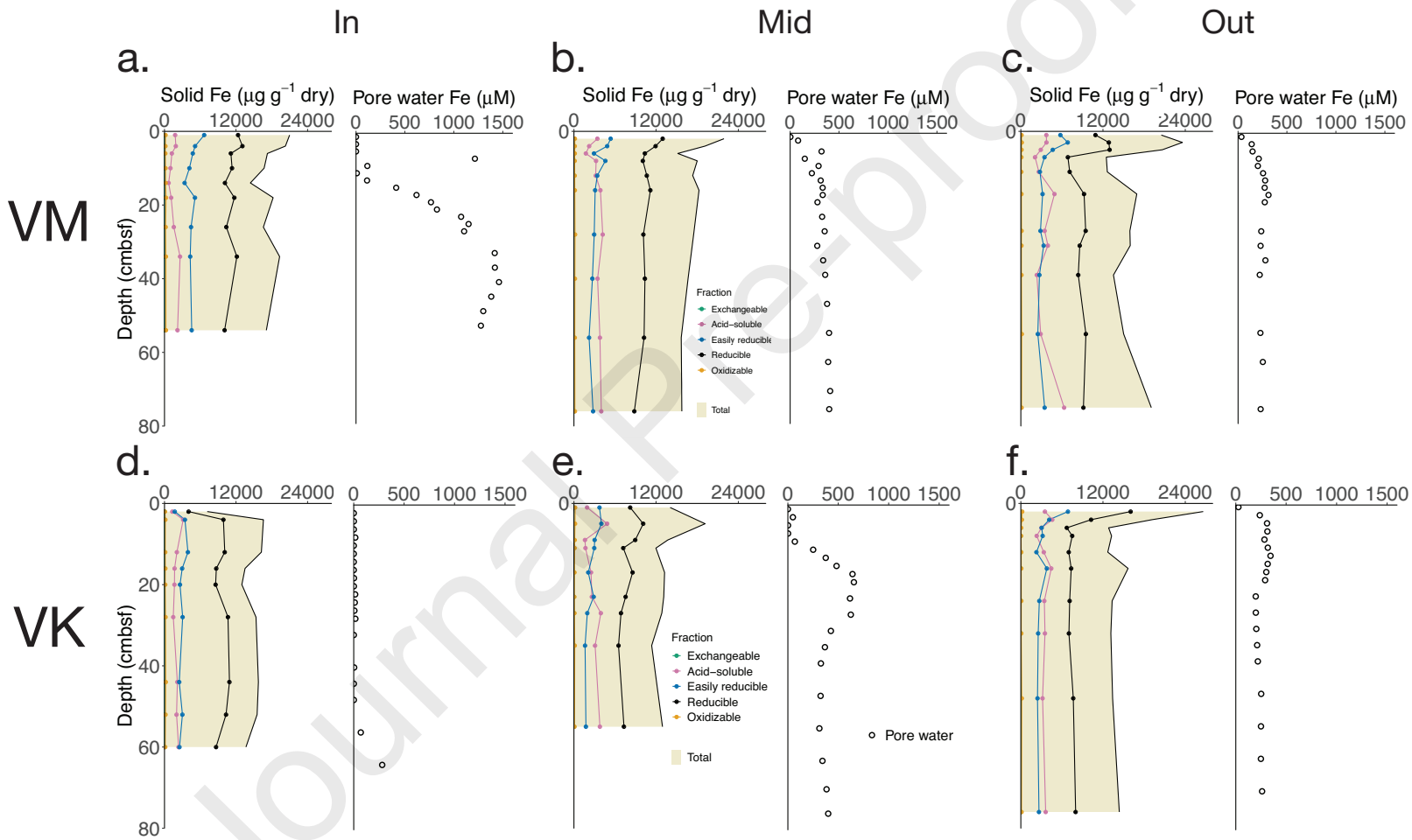


Journal Pre-proofs

# Figure 6

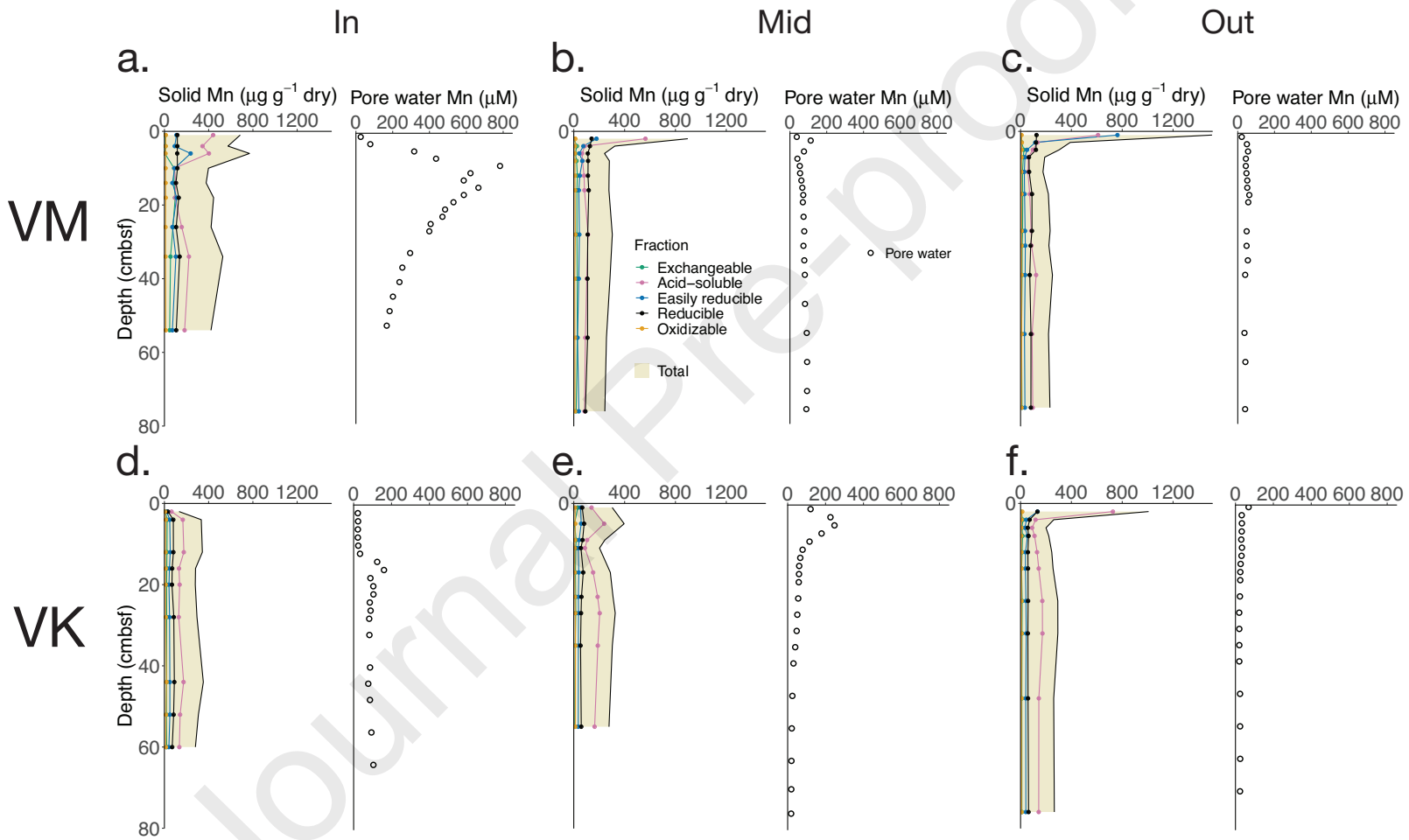


Journal Pre-proofs

Figure 7

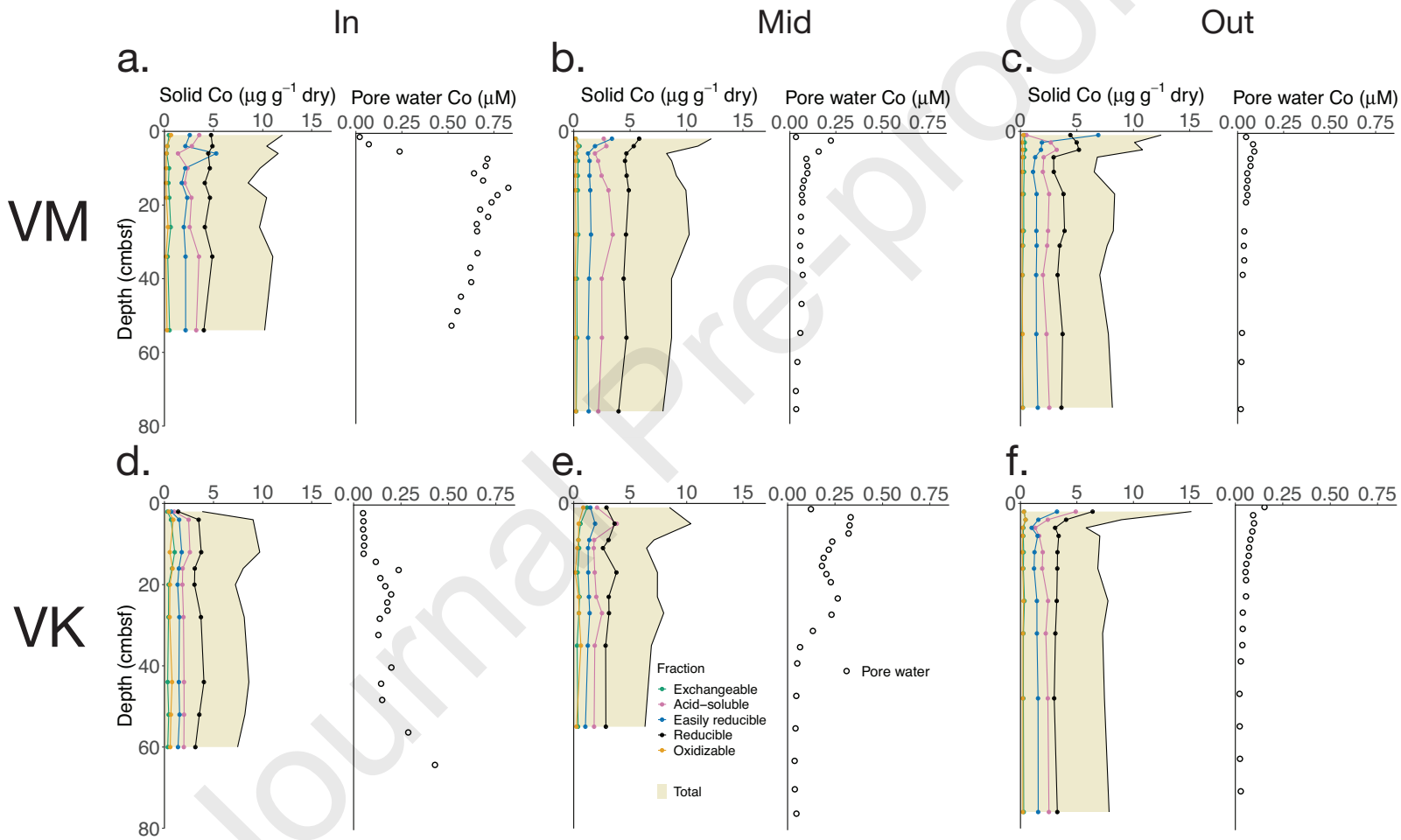


Journal Pre-proofs

# Figure 8

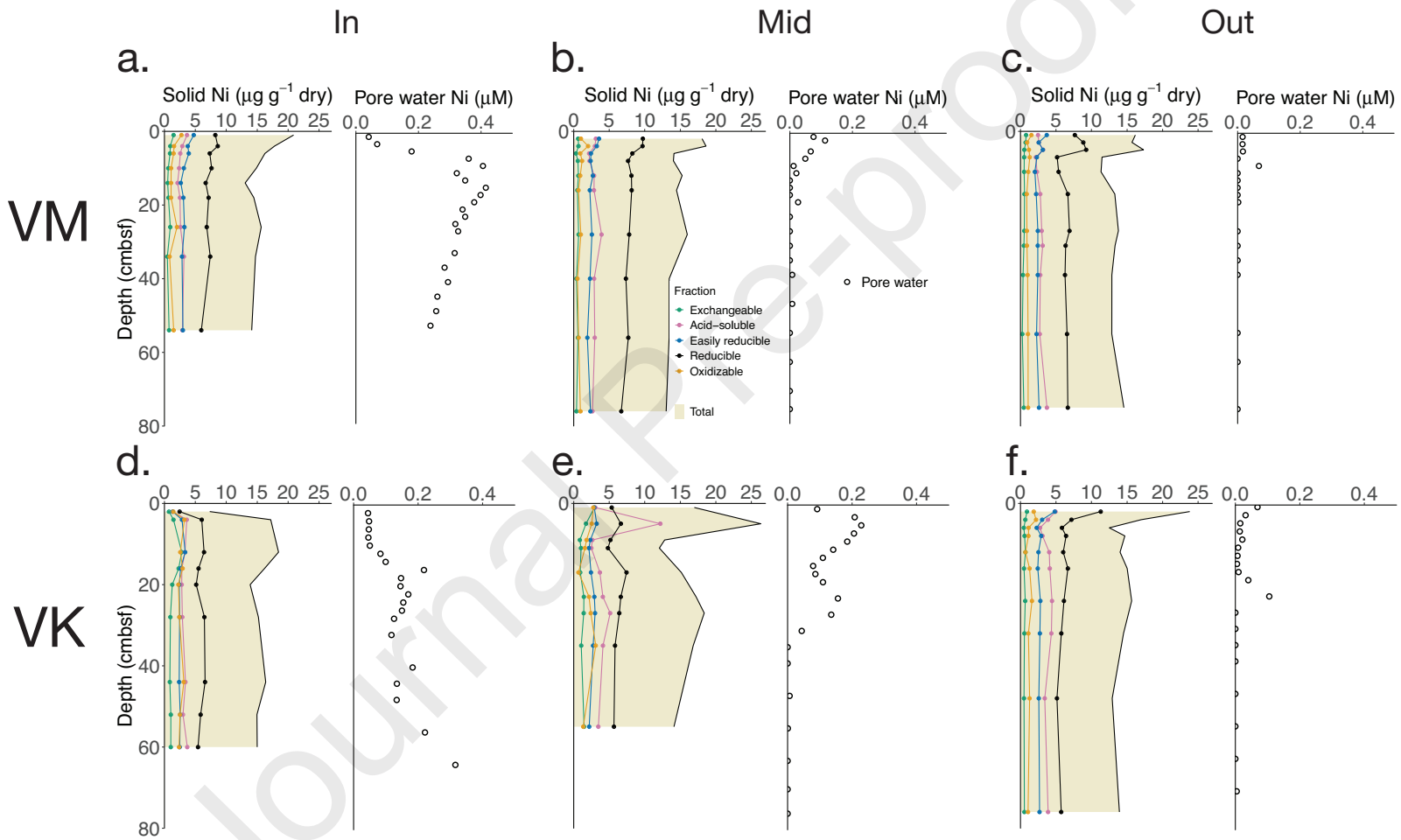


Journal Pre-proofs

Figure 9

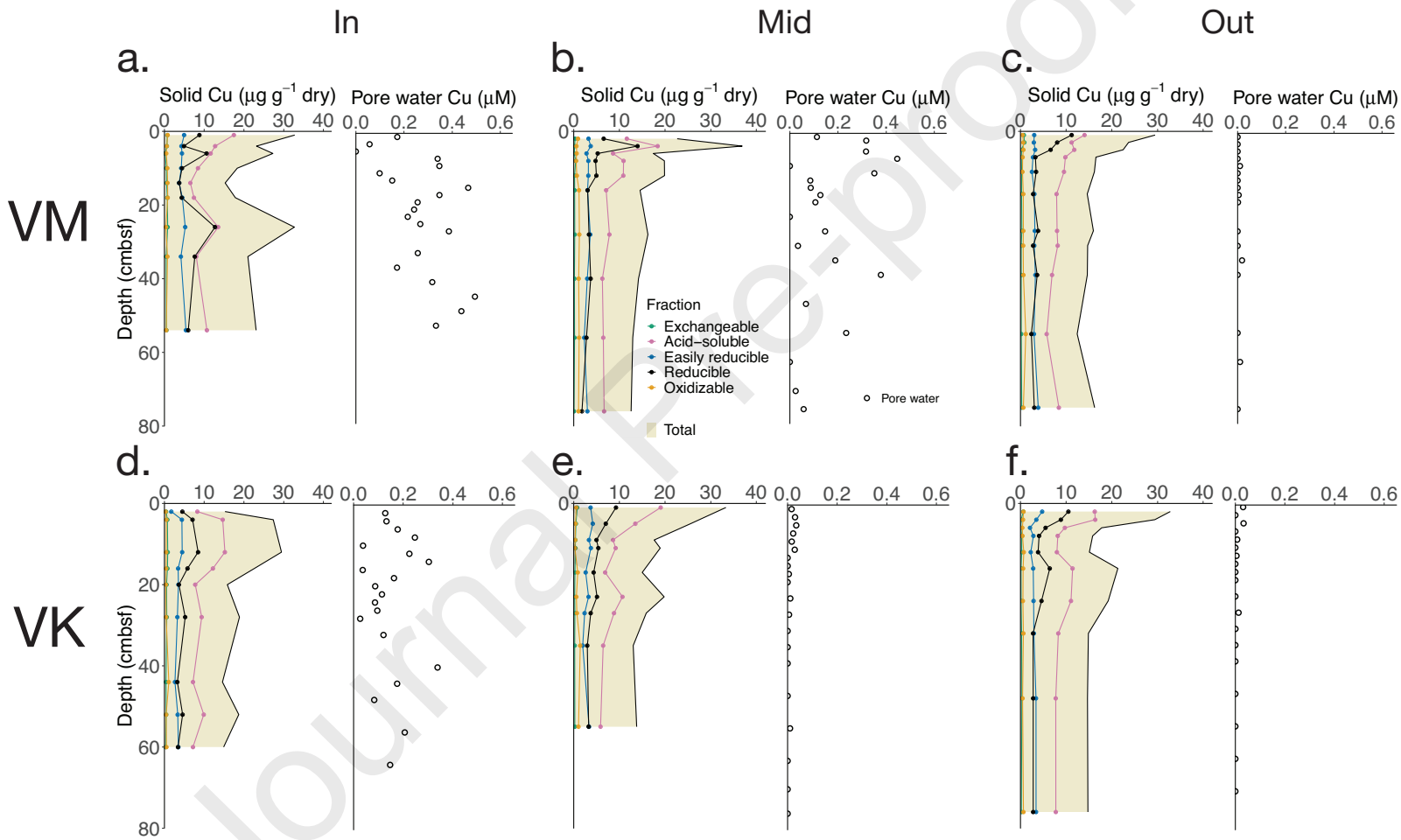


Journal Pre-proofs

Figure 10

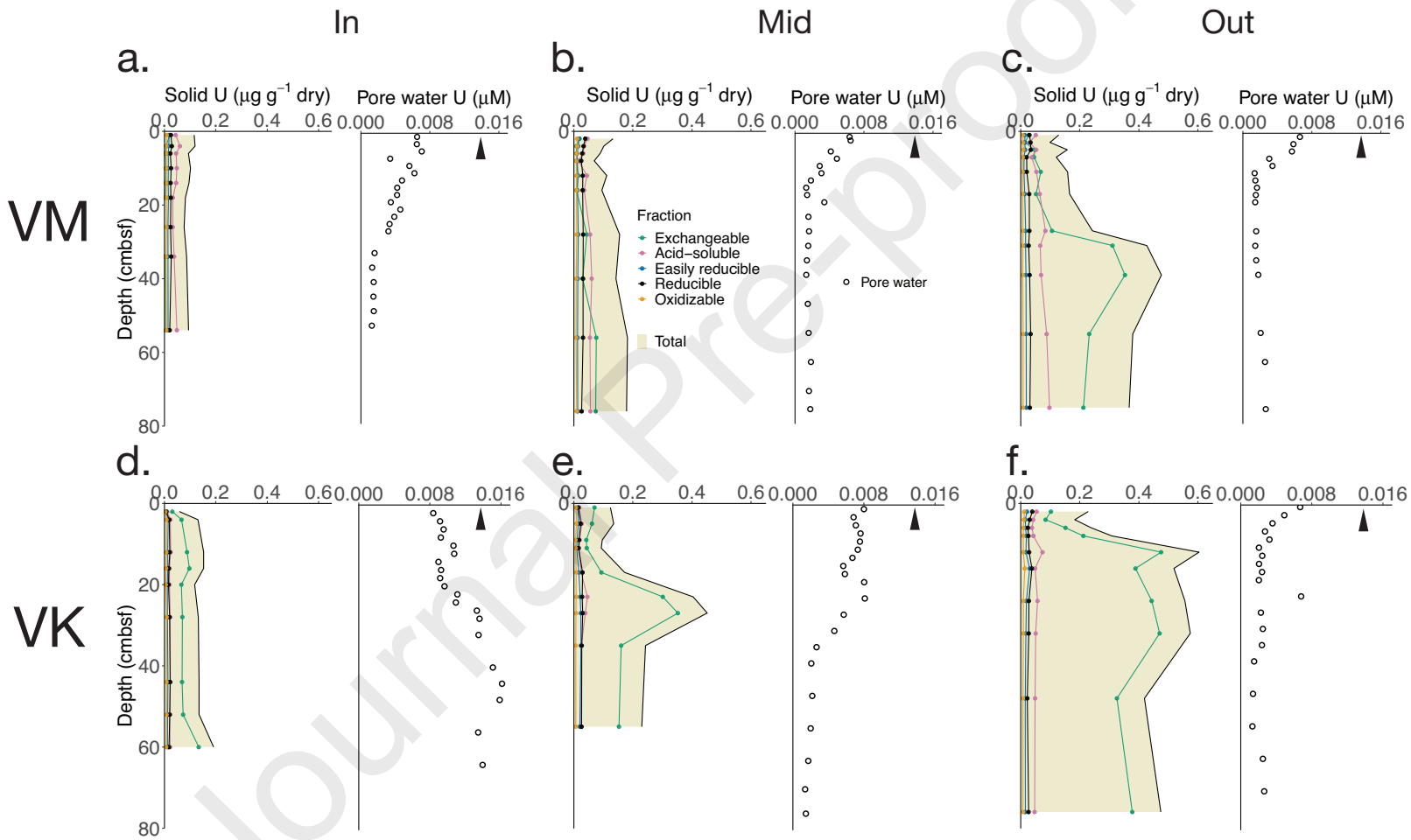


Journal Pre-proofs

# Figure 11

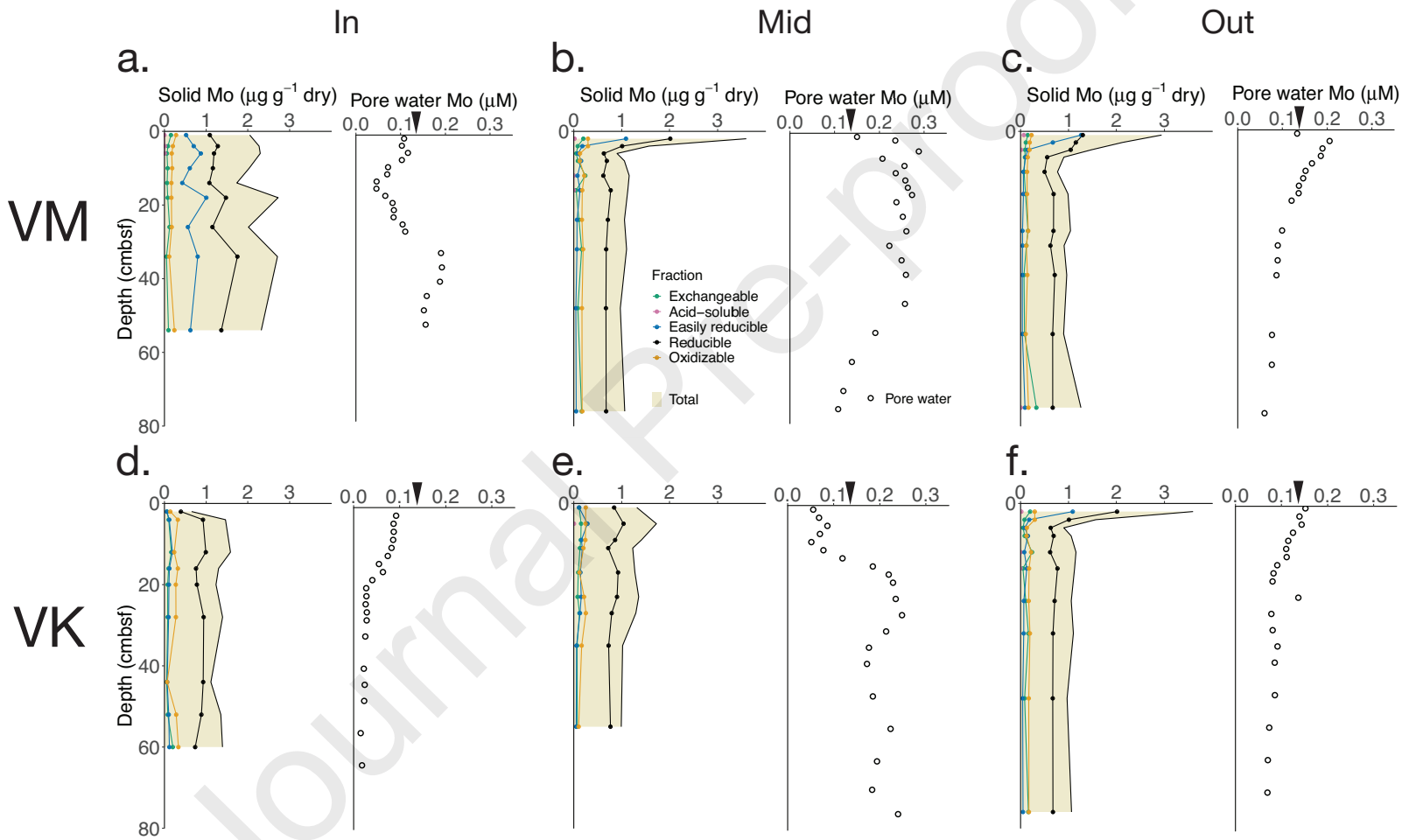


Journal Pre-proofs

Figure 12

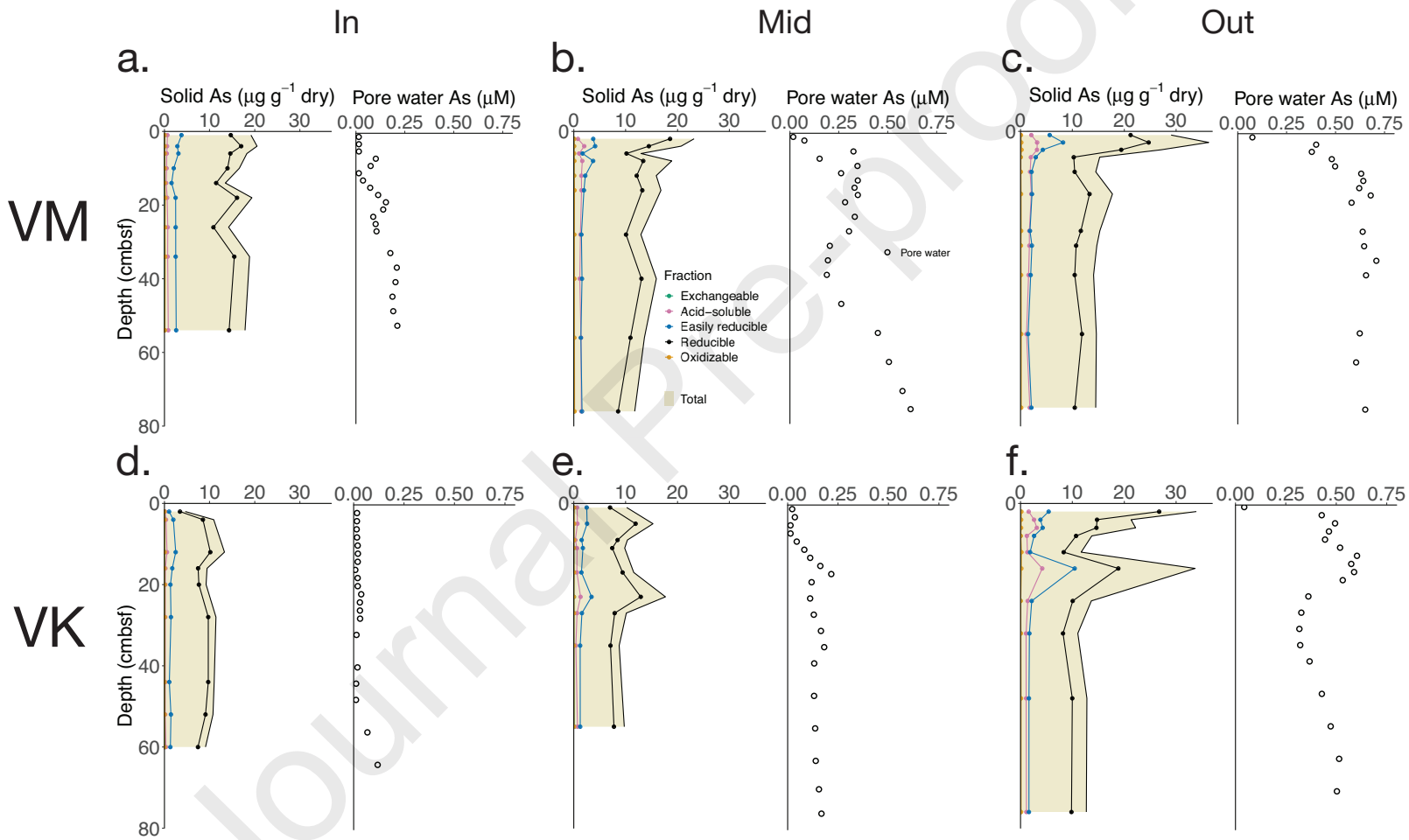


Journal Pre-proofs

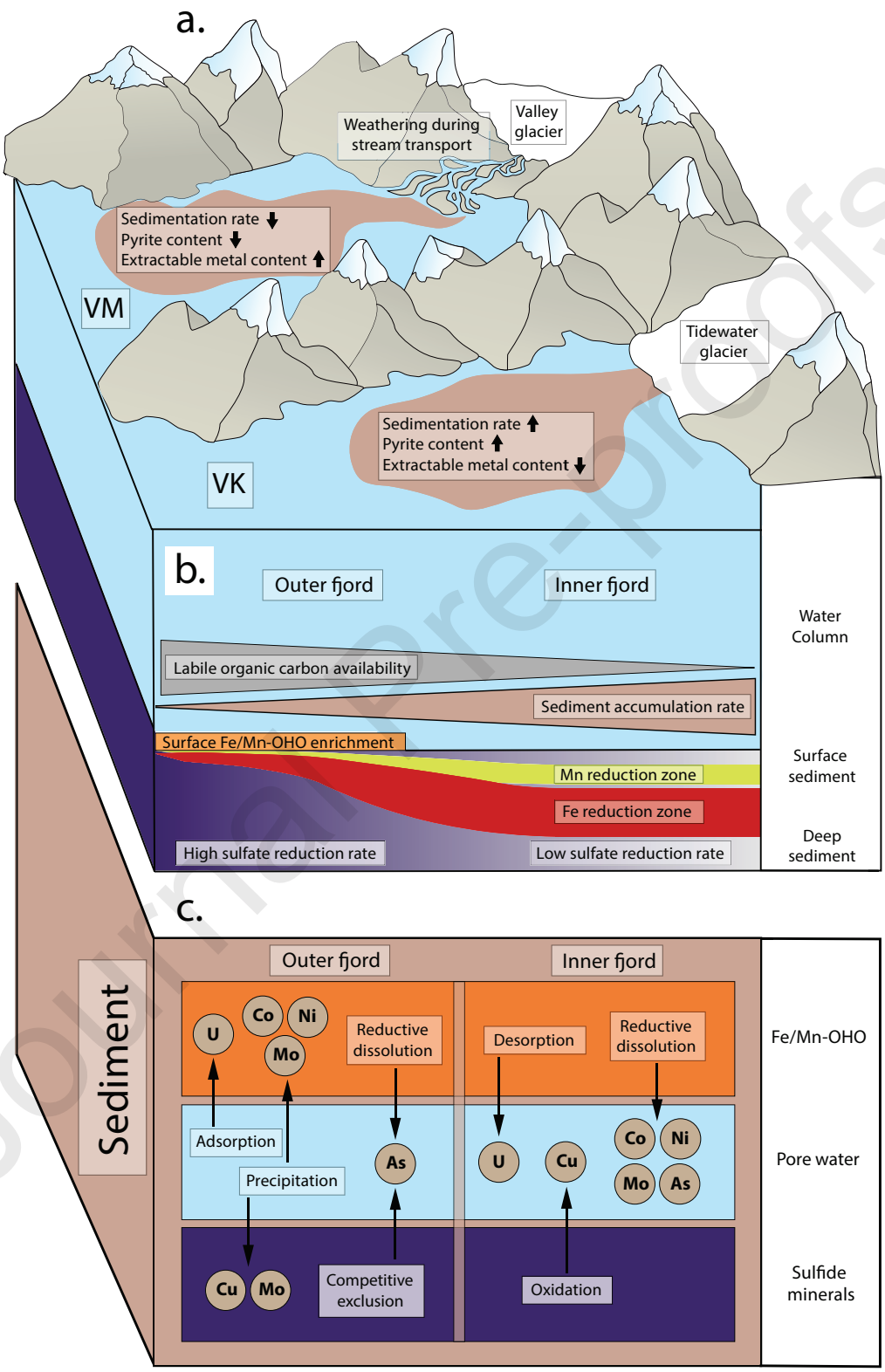


Journal Pre-proofs

**Table 1. Information on size, depth, glacial input, and geology of the fjords sampled in this study.** References: Hjelle, 1993; Wehrmann et al., 2014; http://svalbardkartet.npolar.no. "Program station name" refers to the name of the station given during the sampling expedition, provided here for cross-reference with other data collected during the same expedition. "Station name" is the name given within the context of this paper alone. Note: In the column "Major meltwater inputs," a name ending with –dalen is a valley that was previously glaciated but now funnels a system of meltwater streams, while a –breen is a glacier connected to the fjord by meltwater stream

| Fjord | Length x Width (km) | Tidewater glaciers | Major meltwater inputs | Bedrock lithology | Program station name | Station name | Water depth (m) |
|---|---|---|---|---|---|---|---|
| **Van Mijenfjorden** | 55x10 | Paulabreen | Kjellströmdalen, Reindalen, Berzeliusdalen, Fridtjovbreen | Clastic sedimentary rock, calcareous and dolomitic limestone, shale, sandstone, siltstone, carbonaceous phyllites, coal | AF | VM-In | 63 |
| | | | | | AG | VM-Mid | 69.8 |
| | | | | | AH | VM-Out | 116 |
| **Van Keulenfjorden** | 40 x 7.5 | Nathorstbreen, Doktorbreen | Penckbreen | Clastic sedimentary rock, shale, siltstone, sandstone, dolomite, red conglomerates, chert, arkostic and lithic arenites | HA | VK-In | 25.7 |
| | | | | | AC | VK-Mid | 55.6 |
| | | | | | AB | VK-Out | 100 |

Journal Pre-proofs

**Table 2. Description of the sequential extraction procedure applied in this study.**

| Fraction | Reagents | Chemical Grade | Reference |
|---|---|---|---|
| **Exchangeable** | 1 M $MgCl_2$ | Puratronic 99.999% (metals basis) | Tessier et al., 1979; Heron et al., 1994; Poulton and Canfield, 2005 |
| **Acid-soluble** | 1 M sodium acetate, pH = 4.5 adjusted with acetic acid | Sodium acetate: Puratronic, 99.985% (metals basis) Acetic acid: Glacial, trace metal grade | Tessier et al., 1979; Poulton and Canfield, 2005 |
| **Easily reducible** | 1 M hydroxylamine · HCl | 99.999% trace metals basis | Chester and Hughes, 1967; Tessier et al., 1979; Poulton and Canfield, 2005 |
| **Reducible** | 50g/L dithionite buffered with citrate | Sodium hydrosulfite: Laboratory grade | Mehra and Jackson, 1960; Poulton and Canfield, 2005 |
| **Oxidizable** | 8.8 M $H_2O_2$, pH = 2-3 1M ammonium acetate, pH=2 adjusted w/ nitric acid | Ammonium acetate: 99.999% trace metals basis $H_2O_2$: Suprapur | Gupta and Chen, 1975; Tessier et al., 1979 |

Journal Pre-proofs

**Table 3**. **Average total inorganic carbon (TIC), total organic carbon (TOC), and total organic carbon to total nitrogen ratio (C/N) ± one standard deviation at all sites.**

| Fjord | Site | TIC (wt. % C) | TOC (wt. % C) | C/N (mol $mol^{-1}$) |
|---|---|---|---|---|
| **Van Mijenfjorden** | VM-In | 2.03 ± 0.14 | 1.99 ± 0.14 | 20.4 ± 0.54 |
| | VM-Mid | 1.90 ± 0.11 | 1.83 ± 0.11 | 17.4 ± 1.4 |
| | VM-Out | 1.95 ± 0.09 | 1.82 ± 0.12 | 16.2 ± 0.84 |
| **Van Keulenfjorden** | VK-In | 1.81 ± 0.06 | 1.59 ± 0.06 | 19.1 ± 1.4 |
| | VK-Mid | 2.01 ± 0.12 | 1.58 ±0.12 | 18.3 ± 1.3 |
| | VK-Out | 2.26 ±0.13 | 1.76 ± 0.09 | 17.8 ± 0.99 |

Journal Pre-proofs

**Declaration of interests**

☒ The authors declare that they have no known competing financial interests or personal relationships that could have appeared to influence the work reported in this paper.

☐The authors declare the following financial interests/personal relationships which may be considered as potential competing interests:

Journal Pre-proofs